AN ELECTROHYDRODYNAMIC WICK

Author: David Lee Luck

Thesis
Supervisor: Prof. J. R. Melcher

Date
Submitted: May 23, 1969

AN ELECTROHYDRODYNAMIC WICK

by

DAVID LEE LUCK

LIEUTENANT, UNITED STATES NAVAL RESERVE

B.S., OHIO UNIVERSITY

(1963)

Submitted in Partial Fulfillment of the

Requirements for the Degree of

Naval Engineer and the Degree of

Master of Science in Electrical Engineering

at the

MASSACHUSETTS INSTITUTE OF TECHNOLOGY

May, 1969

AN ELECTROHYDRODYNAMIC WICK

by

DAVID LEE LUCK

Submitted to the Department of Naval Architecture and Marine Engineering and the Department of Electrical Engineering in partial fulfillment of the requirements for the Degree of Naval Engineer and the Degree of Master of Science in Electrical Engineering

ABSTRACT

A simple, easily fabricated geometry is proposed for arrays of ion drag pumps to be used in a wick configuration for electrical pumping of dielectric fluids to arbitrary heights. Static and dynamic models for pumping are presented and compared with experimental measurements for the proposed geometry. A pressure oscillation as predicted by the theory and observed experimentally is investigated and the adequacy of the dynamic model is evaluated. Design parameters for an electrohydrodynamic wick are defined, and the performance of an experiment wick is presented.

THESIS SUPERVISOR: James Russell Melcher

TITLE: Associate Professor of Electrical Engineering

AN ELECTROHYDRODYNAMIC WICK

by

DAVID LEE LUCK

Submitted to the Department of Naval Architecture and Marine Engineering and the Department of Electrical Engineering in partial fulfillment of the requirements for the Degree of Naval Engineer and the Degree of Master of Science in Electrical Engineering.

ABSTRACT

A simple, easily fabricated geometry is proposed for arrays of ion drag pumps to be used in a wick configuration for electrical pumping of dielectric fluids to arbitrary heights. Static and dynamic models for pumping are presented and compared with experimental measurements for the proposed geometry. A pressure oscillation as predicted by the theory and observed experimentally is investigated and the adequacy of the dynamic model is evaluated. Design parameters for an electrohydrodynamic wick are defined, and the performance of an experimental wick is presented.

THESIS SUPERVISOR: James Russell Melcher

TITLE: Associate Professor of Electrical Engineering

Acknowledgements

I wish to acknowledge the guidance of Prof. James R. Melcher, whose efforts made this exercise a meaningful learning experience.

In addition, I appreciate the efforts of my wife Sandy in typing the thesis, and her patience during my hours of study.

This work was supported under NASA grant number NGL-22-009-014.

Table of Contents

INTRCDUCTION

A conventional wick employs surface tension to raise fluids against gravity and is used in applications where only small flow rates are required. The wick is extremely simple and reliable and requires no external source of power. An example of current interest where a conventional wick is applied is in the liquid return path of a heat pipe. Heat pipes are used in many applications where large quantities of heat must be removed from a confined space. Examples include heat transfer from the core of a nuclear reactor, the cooling of large electronic tubes and semiconductor components, and heat removal from transformers. Heat is picked up by the working fluid of the heat pipe as latent heat of vaporization when the liquid evaporates and is convected along with the vapor until the liquid condenses in the condensor section and the heat is rejected to some heat sink. The liquid must then be returned to the evaporator in order that the cycle be continuously repeated and this is usually accomplished with a conventional wick. Using this process, heat fluxes can be achieved which are much higher than those possible by conduction through a metallic conductor with the same temperature difference between the heat source and sink. The limitations upon heat transfer rate which can be achieved with a heat pipe

fall into two areas: first, the flow rate of the liquid returning from the condensor to the evaporator is limited if a conventional wick is used as the return mechanism; second, the heat flux in the evaporator is limited because of the vapor film which forms at the liquid-metal interface and acts as an insulator to increased heat flux.

Limitations on flow rate in the conventional wick occur because of the competing effects of surface tension and viscous drag. Liquid will rise through the pores of the wick until the surface tension force at the liquid surface balances the gravitional body force on the liquid in the pore. To increase the potential heighth to which the liquid can be raised, the average pore diameter of the wick must be decreased to increase the ratio of liquid-solid interface to cross sectional area. As the fluid begins to flow the surface tension forces must compete with another pressure loss due to viscous drag. Viscous drag increases as the diameter of the pores are decreased. Hence for a given heighth to which the fluid must be raised, there is a limited flow rate which can be realized.

An increase in liquid flow rate by using an independent pumping mechanism could provide an increase in the heat transfer capability of a heat pipe. However one of the attractions of the conventional heat pipe is that the wick pumping does not require an independent energy source and is highly reliable. But if the energy source used for pumping

could also be used to help overcome the other limitation on the heat pipe performance, i.e. the maximum heat flux due to film boiling in the evaporator and condensation in the condensor, improvement of the total performance of the heat pipe becomes an attractive possibility.

There has been investigation of improvement in evaporation and condensation heat flux by using electric fields to cause the vapor film to become unstable and break away from the metal boiler or condensor surface. This requires a high voltage source and suggests that if such a scheme could be applied to the heat pipe, a natural area of investigation toward improvement of the total heat pipe performance would be the use of electric fields to provide the pumping force for the working liquid.

The use of electric fields in pumping of liquids can take advantage of either dielectrophoretic force where the force is perpendicular to the electric field direction, or the body force on the fluid due to the ion drag phenomenon where the force is in the direction of the applied field. In either case the fluid must be a good insulator and should resist electrical breakdown as well as possible because the forces exerted increase as the field increases. A fluid satisfying these requirements is freon 113 which is used widely as a heat transfer agent.

The requirements of the pumping mechanism for the heat

pipe application are these:

(1) It must be possible to achieve high flow rates relative to those possible with a conventional wick.

(2) It must be possible to raise the liquid to an arbitrary heighth in a gravitational field or to move the liquid against adverse accelerations such as those encountered in a space application.

(3) The pumping mechanism must be highly reliable.

(4) Simplicity and ease of fabrication are necessary if it is to compete with a conventional wick.

The use of dielectrophoretic force for pumping fails on the second requirement above. The maximum pressure which can be generated at the interface of a liquid is $\frac{1}{2}(\epsilon - \epsilon_0)E^2$ where ϵ is the permittivity of the liquid and ϵ_0 is the permittivity of the space adjacent to the liquid surface. For freon this pressure represents less than 6 centimeters head for the maximum field which can be tolerated without electrical breakdown. In addition no convenient method of staging the pumps is available; hence the pressure rise achieved in separate stages cannot be added. Thus the maximum vertical dimension of a heat pipe using this method of pumping would be less than 6 centimeters if the condensor were located below the evaporator. Such a limitation would not be imposed in a space application but the adverse accelerations under which the pipe could operate would be limited.

The remaining possibility for application of electrical

pumping is that of the ion drag phenomenon. Investigation of this phenomenon has been made most recently by Stuetzer (1,2,3) and Pickard.[5] A practical pump has been suggested and patented by the former and has been used to achieve high pressure rised in the fluids investigated. However the geometries used are quite difficult to fabricate especially in the numbers that would be required for the heat pipe wick application. In fact the requirement of this application is to achieve high flow rates; pressures need be only high enough to lift the liquid to the next stage of the pump. Therefore a simple geometry for ion drag pumping which permits high flow rates and adquate pressures is the basic requirement of this application. Proposal and investigation of such a geometry is the subject of this thesis.

The ion drag phenomenon can be characterized as follows: A body force can be exerted on an insulating fluid if charged particles in the fluid are pulled along by an electric field. The particles transfer momentum to the fluid through friction as they move under the influence of the electric field, and a pressure gradient is generated in the fluid which results in a pumping motion if the fluid is permitted to move. The magnitude of the pressure which can be realized is limited by the electrical breakdown strength of the fluid. A typical arrangement is one in which two electrodes are used, one being a point at which corona discharge produces the necessary charged particles and the other electrode being more

blunt so that few charged particles are produced there. When a sufficiently high voltage is placed between the electrodes, a pressure gradient is generated and pumping of the fluid will usually occur from the point to the blunt electrode if the flow geometry permits. In order to produce pressures large enough to be of interest, it is necessary to provide lateral boundries of insulating material between the electrodes to insure that most of the charged particles flow in the desired direction of pumping.

Because of the requirement for lateral boundries in the ion drag pump the physical size of a single pump is usually quite small and therefore the flow rate which can be realized is not large. In addition, the physical geometry of the pump provides a large hydrodynamic resistance factor which produces a pressure loss depending upon the flow rate. As the flow rate increases the point at which the pressure loss exceeds the generated pressure is soon reached.

In order to make practical use of ion drag pumps for the wick application to a heat pipe, it is necessary that one be able to fabricate large numbers of these pumps in parallel to achieve the necessary flow rates. Also since we must sacrifice a large percentage of generated pressure to hydrodynamic losses in the pump itself, an arrangement for placing the paralleled arrays of pumps in series is necessary. Since the objective is to use the entire arrangement as a wick, the resultant pressure from each stage need be only slightly great-

er than necessary to raise the fluid vertically through the pump dimension and to the next stage. Therefore a geometry will be sought which maxumizes flow rate while maintaining sufficient pressure to operate as a wick.

Finally the objectives of provision for parallel and series operation must be achieved with a geometry which can be easily fabricated and whose dimensions may be easily adjusted to achieve the desired tradeoff between pressure and flow rate.

The possible application of an electrohydrodynamic wick satisfying the given requirements is not limited to heat pipes. However it was this application which provided the motivation for study. Another possible application would be to provide motion of the oil inside transformers thus eliminating hot spots. Tom Jones has used the configuration presented in this thesis in a wall-less pipe.(7)

The ion drag pumping of liquids has been observed for many years but little application has been made of the phenomonen. With the wick application to heat pipes in mind, the goal of this investigation has been to develop a configuration so simple it could be made and used by anyone having requirement for a similar pumping device, and to determine the characteristics of the device sufficiently well that a systematic design can be made for any required application.

CHAPTER I

PUMP GEOMETRIES

Pump Geometries Investigated

The geometry investigated in most experiments reported by Stuetzer[1] was that of a point to ring as shown in figure I-1. Corona discharge at the point electrode produces free charge which is pulled toward the ring electrode and the fluid is pumped in the direction shown. High pressure rises in the fluid can be realized across the pump. The disadvantage of this geometry is that fabrication of many of these pumps is difficult because point electrodes must be placed within the channel at a precise distance from the ring. In addition the point electrode and its support provides an additional hydrodynamic resistance to the flow. This is significant for the present application because the object is to operate at low pressure rise and high flow rates.

The geometry used by Pickard in his investigation was that of two grids of thin wire across the channel as shown in figure I-2. The same effect can be achieved by using wire screens. These offer hydrodynamic resistance to the flow; in addition, wire or screen fine enough to act as a corona emitter is easily broken and makes fabrication difficult.

Other geometries were investigated including the straight wire to ring configuration shown in figure I-3. Here the charges are produced near the thin wire and the fluid is pumped toward the ring electrode. This geometry is easier to fabricate than the point to ring since the same wire can be placed across the channels of adjacent pumps in

parallel. However the electric field configuration is not symetric about the channel axis being stronger at the sides near the wire and weaker 90 degrees from this point around the channel. Circulation of the fluid between the electrodes occurs before the pressure developed is as high as desired.

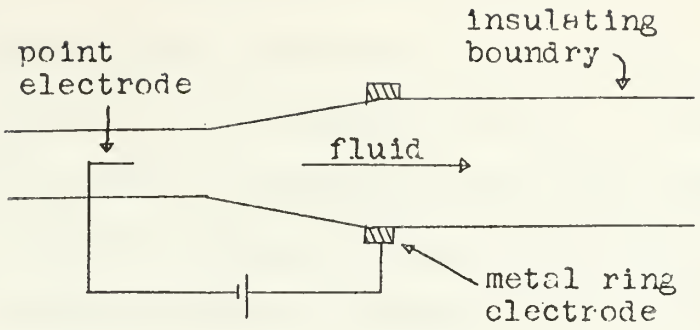

Point to Ring Geometry

Figure I-1

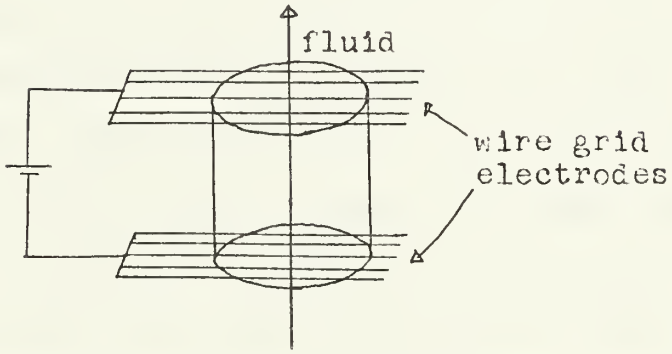

Grid Electrode Geometry

Figure I-2

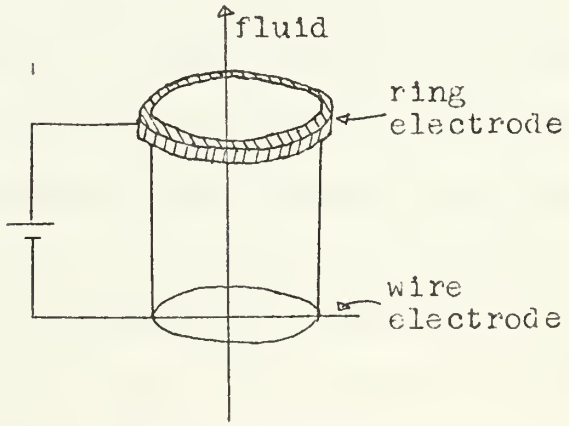

Line to Ring Geometry

Figure I-3

Proposed Pump Geometry

The pump geometry which was selected and tested is as shown in figure I-4. It consists simply of two thin metal plates with a sheet of plexiglas sandwiched between. To make the pump, a hole is drilled through the metal plexiglas sandwich. As the drill bit emerges from the first brass sheet and enters the plexiglas, a burr or projecting sharp edge is formed. In freon, testing has shown that this is sufficient to produce the necessary free charge as ions within the liquid. The channel through the plexiglas directs the ions such that their motion toward the other electrode causes a pressure to be built up between points (A) and (B) in figure I-4. The electrodes are secured to the plexiglas before the hole is drilled so that the pump need not be realligned after drilling. The extreme simplicity of the geometry makes it easy to produce pumps with a variety of electrode spacings (by changing the hole size). By doing so it is possible to determine optimum dimensions to produce the best performance with respect to pressure and flow rate.

Parallel operation of pumps is easily produced by drilling several holes as shown in figure I-5. The possible interaction of pumps which might degrade performance was investigated to determine if a minimum spacing of the pumps is required. It was also necessary to determine if slight differences in electrode edges would degrade the overall performance of the entire array.

The series arrangement is shown in figure I-6. It consists of several layers of the parallel arrays. The regions between the arrays are reservoirs for the liquid. On either side of these reservoirs are exposed electrodes of opposite polarity and placed such that they would cause a loss in pressure if ions were pulled across this space in opposition to the desired flow direction. However, since there are constricting boundries as there are in the pump region, little loss was observed. In any case, such loss can be decreased by increasing the spacing between pump arrays.

One difficultity with the given pump geometry is that it is not easy to analyze mathematically. It does not fall exactly into any of the three catagories analyzed by Stuetzer,[1] i.e. plane, cyclindrical, or spherical. The emitter electrode is not a plane surface, a point, or a straight line but a ring at one end of the cyclinder. Therefore it is necessary to base the analytical model on an approximate geometry. Experimental study of the actual pump was used to determine what adjustments were necessary to the mathmatical model in order to have reasonable predictions of performance to be used in design of practical wick arrays for a specific application.

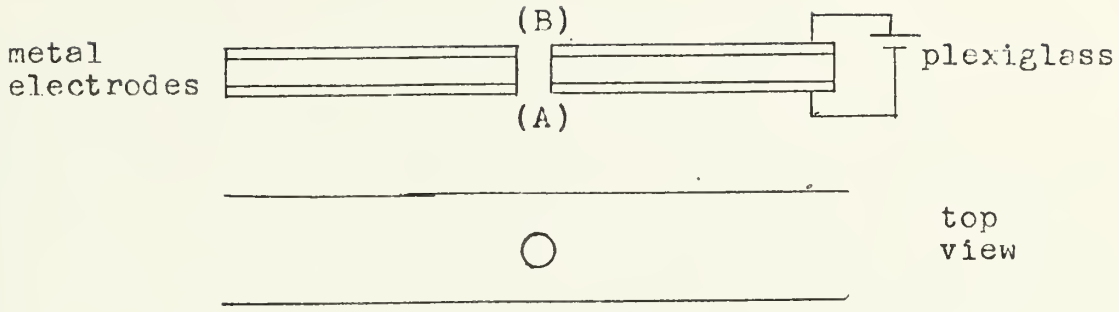

Single pump

Figure I-4

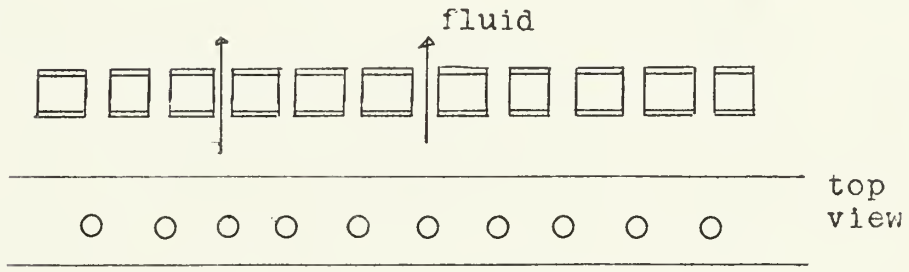

Array of pumps in parallel

Figure I-5

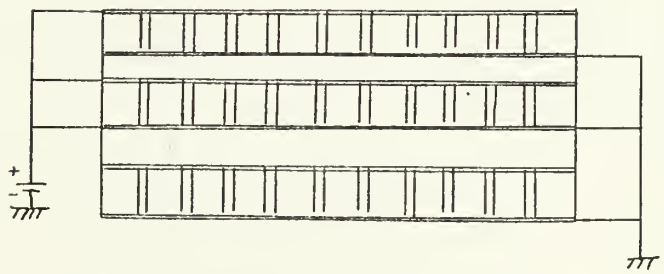

Pump arrays in series

Figure I-6

CHAPTER II

STATIC PRESSURE GENERATION

Static Pressure Generation

The static model for the ion drag device relates the external fluid pressure generated with the applied voltage since the device will be driven by a constant voltage d.c. source. The geometry explained in chapter I is complicated to model analytically. Therefore development of the model will be done as follows. Experiments have shown that for a particular set of pump dimensions the pressure-voltage dependence can be modeled by a space charge limited current and the problem can be solved if a simple geometry is chosen as done by Stuetzer[1]. This theory is then modified to account for the observed performance of the proposed pump geometry. Experiment has also shown that there is a dependence of generated static pressure upon the transverse dimensions of the pump. This dependence was investigated experimentally to determine optimum dimensions for wick application.

One Dimensional Static Model

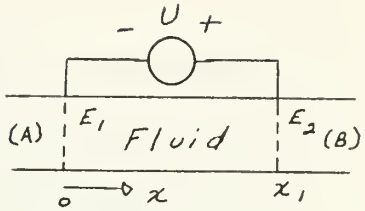

Figure II-1

A one dimensional model as shown in figure II-1 will be assumed. The charged particles enter the fluid at the electrode E_1 and are removed from the fluid at electrode E_2. Therefore the charge relaxation time of the liquid must be greater than the transient time of the particles between electrodes. The electric field seen by the particles will be the macroscopic field of the system and individual particles will not influence one another. The liquid will appear as a continuum to the moving particles. It is assumed that only one type of charged particle is present. This can be realized if the electrodes are not symmetrical or if the fluid exhibits a strong tendency to produce only one type ion in a corona discharge. The electrical force on a particle will be

$$F_p = qE$$

where q is the particle charge and E is the local field at the particle. The viscous force exerted on the particle by the fluid is proportational to the velocity of the particle relative to the stationary fluid

$$F_v = \gamma v$$

The particle velocity can be expressed in terms of the electric field since the viscous and electrical forces must balance in steady motion

$$v = \frac{F_v}{\gamma} = \frac{F_p}{\gamma} = \frac{qE}{\gamma} = bE$$

The quantity b is called the mobility and will be assumed independent of the field. If the fluid is stationary and charge diffusion is neglected the current then can be expressed as

$$j = \rho v = \rho b E \qquad (1)$$

where ρ is the charge density and j is the current density. The total body force exerted on the fluid per unit volume is the total electric force

$$f = \rho E$$

Since the fluid is not in motion there are no inertial or viscous forces and the body force must be balanced by a pressure gradient.

$$\rho E = \nabla p \qquad (2)$$

Surface charges on the circumference of the channel will be neglected. Hence the charge density and the electric field will be uniform across the channel and the electric field will have only an x component. Gauss's Law is then written

$$\frac{dE}{dx} = \frac{\rho}{\epsilon} \qquad (3)$$

and the electric field is related to the voltage through

$$\frac{du}{dx} = -E \qquad (4)$$

Substitute (3) into (1)

$$\frac{j}{\epsilon b} = E \frac{dE}{dx}$$

and integrate from $x = o$ to x and $E = E_e$ to E

$$\frac{j}{\epsilon b} x = \frac{1}{2}\left(E^2 - E_e^2\right)$$

or

$$E(x) = \left(\frac{2qx}{\epsilon b} + E_e^2\right)^{1/2} \tag{5}$$

From eq. (3) $\rho = \epsilon \frac{dE}{dx}$

$$\rho(x) = \frac{q/b}{\left[\frac{2qx}{\epsilon b} + E_e^2\right]^{1/2}} \tag{6}$$

To find p integrate from $x=0$, x and $p=0$ to p

$$\frac{dp}{dx} = \rho E = \frac{q}{b}$$

$$p = \frac{qx}{b} \tag{7}$$

To introduce voltage integrate eq. (5) using eq. (4)

$$\frac{dU}{dx} = E = \left(\frac{2qx}{\epsilon b} + E_e^2\right)^{1/2}$$

$$U = \frac{\epsilon b}{3q}\left(\frac{2qx}{\epsilon b} + E_e^2\right)^{3/2}$$

$$U = \frac{\epsilon x}{3p}\left(\frac{2}{\epsilon} p + E_e\right)^{3/2}$$

Specific Emitter Assumption

If it is now assumed that $E_e = 0$. This assumption will be discussed later. Then

$$\rho = \frac{q}{8} \epsilon \left(\frac{U}{x}\right)^2 \tag{8}$$

Equation (8) shows that the pressure difference between points (A) and (B) in figure II-1 is independent of the lateral dimension of the channel. This is because the space charge is uniformly distributed across the channel and there are no field components perpendicular to the x direction.

Comparison of equation (8) to the result obtained by Stuetzer [1] for a spherical (point to ring) geometry shows that for a fixed set of pump dimensions, the relationships differ by only a constant. Since an exact relationship cannot be obtained for the geometry proposed in chapter I, a relationship of the following form is assumed;

$$P = C\epsilon\left(\frac{U'}{x}\right)^2$$

where the value of C is to be determined by experiment. In terms of pressure head

$$h = \frac{C\epsilon}{\rho g}\left(\frac{U'}{x}\right)^2 \qquad (9)$$

where h is the head developed across the pump. Here the voltage U' is the difference between the applied voltage and a "cut in voltage" usually taken as the minimum voltage necessary to produce unipolar ionic conduction.

The dependence of pressure proportational to voltage squared is a result of the boundry condition assumption that the electric field at the emitter is zero. Figure II-2 shows a plot of pressure head developed across a pump as a function of U^2. This linear relationship is typical for most pumps investigated in the region of voltage where the pumps are to be operated. Breaks have been observed in these plots but these will be discussed more in chapter V.

The value of C in equation (9) is determined from a plot such as figure II-2 from the equation

$$C = 7.24 \quad x^2 \frac{dh}{dU^2} \tag{10}$$

where x is the electrode spacing in millimeters, $\frac{dh}{dU^2}$ is the slope of the pressure-voltage squared plot in centimeters/(kilovolt)^2.

The value of C depends upon the diameter of the hole and the size of burr produced in drilling. However, it has been found that for most pumps with spacers of 1/16 inch and holes of diameter approximately 1.40 millimeters, the value of C is in the range 0.8 to 1.1 .

The spacing of 1/16 inch was found to work quite well at reasonable voltages of 10-15 KV. Smaller spacings cause electrical breakdown at voltages only slightly above the "cut in voltage" and thicker spacers required extremely large voltages (25-30 KV) to give significant pressures. At the spacing of 1/16 inch breakdown would usually occur at 16 to 19 KV depending upon the purity of the freon.

Pressure Head vs.

Voltage squared

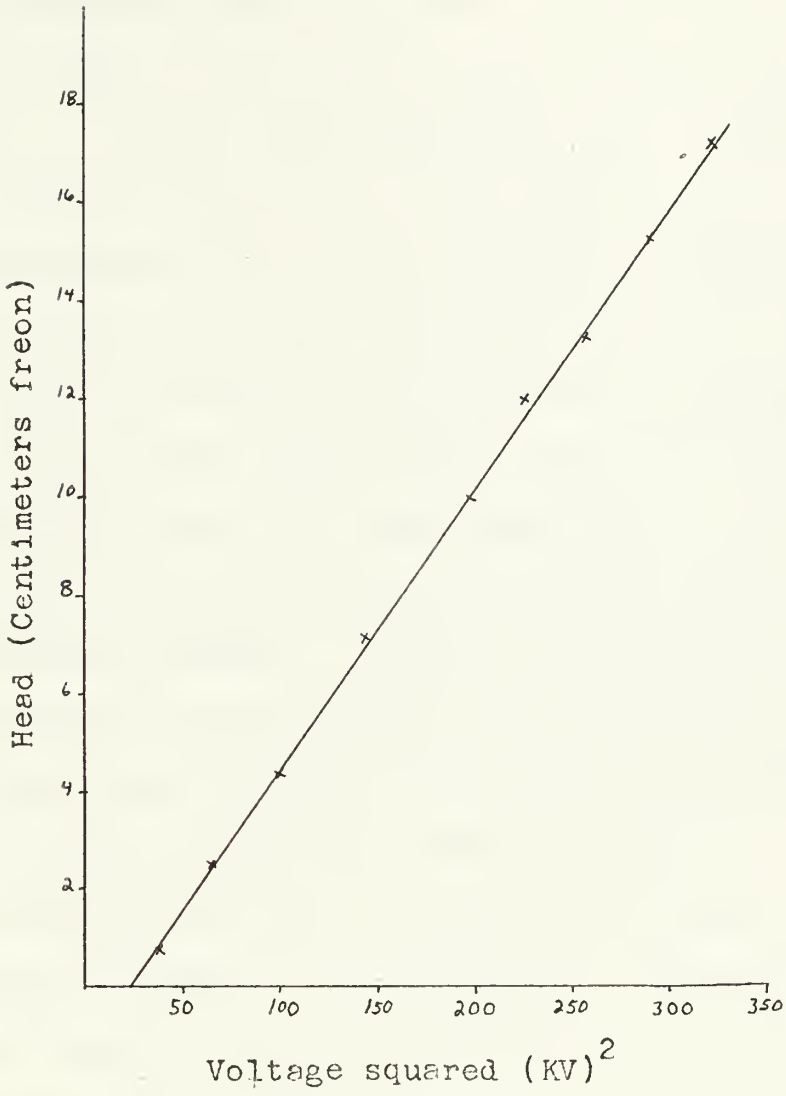

Figure II-2

Experimental Effects of Lateral Pump Dimensions

The preceeding development does not account for any pressure dependence upon the lateral dimension of a pump, i.e. the diameter of the hole for the geometry as proposed in chapter I. As has been stated the exact theoretical solution for this geometry has not been worked out so an experimental investigation was carried out for a large range of hole sizes with pump length fixed at 1/16 inch. Figure II-3 shows a plot of pressure vs. pump diameter at three different voltages for constant pump length. The freon used in these experiments was doped with copper napthenate.

For very large holes the generated pressure decreased with increasing diameter. Ions are being injected only at the outside edges of the channel and it would be expected that for very large diameters the pressure due to drag of the ions toward the collector would be small.

The interesting result is shown by the jump in pressure at a diameter of about 1.9 millimeters. For holes smaller than approximately 1 mm. the pressure does not change much in these experiments. It is not practical to make holes smaller than about 0.2 mm with drill bits which are readily available.

The important conclusion from this investigation is that the optimum regime of operation is around 1 to 1.2 mm diameter. Smaller holes will yield little increase in generated pressure.

Pressure Head vs.

Pump Diameter

(pump length constant 1/16")

Figure II-3

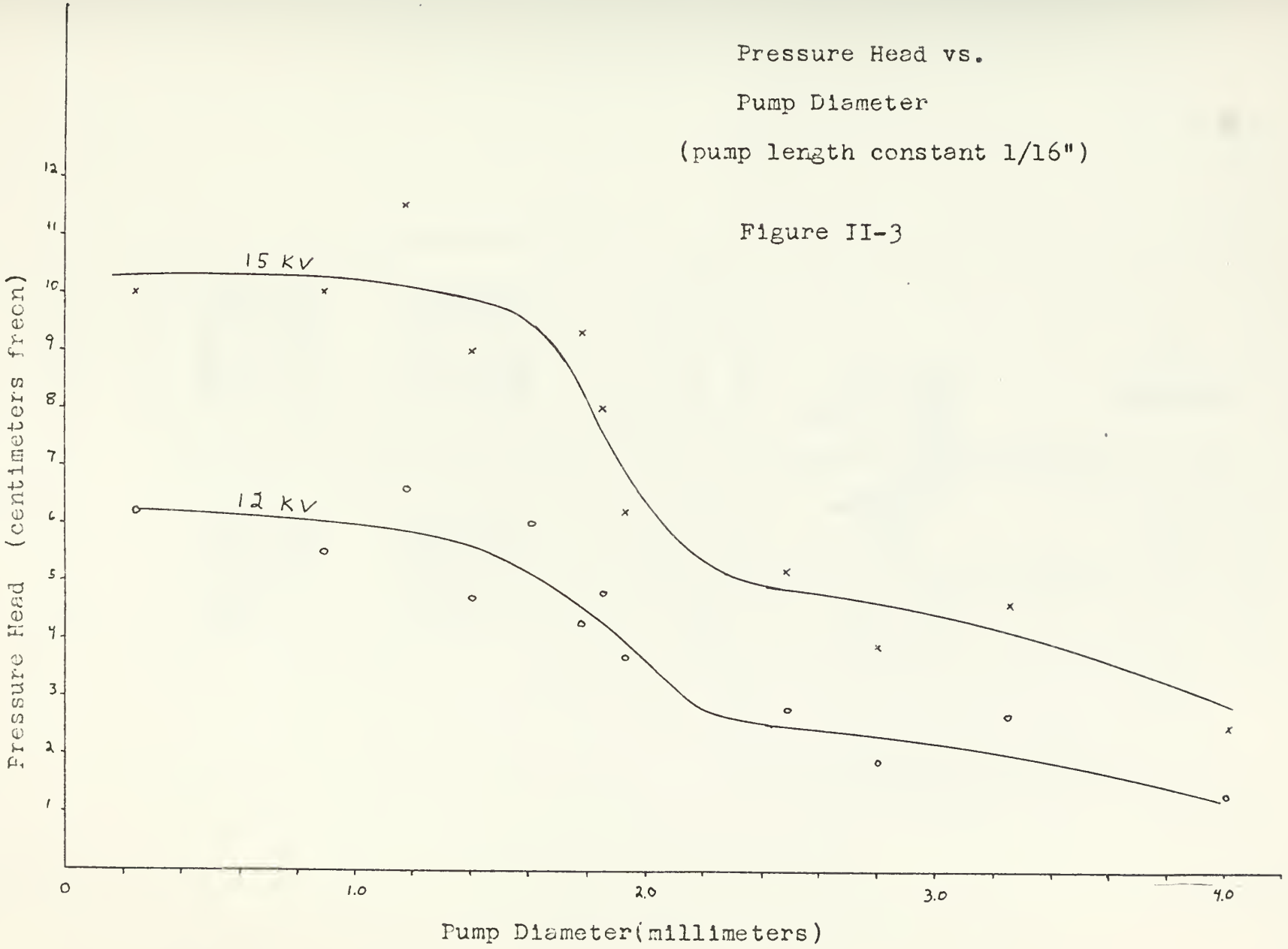

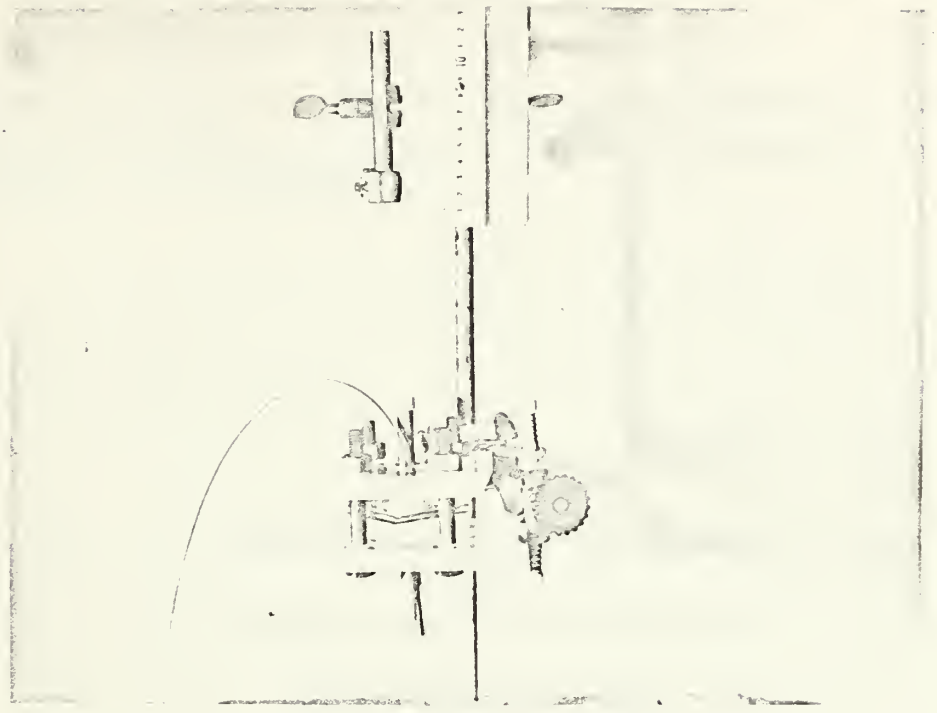

Pump enclosure and manometer used in static tests.

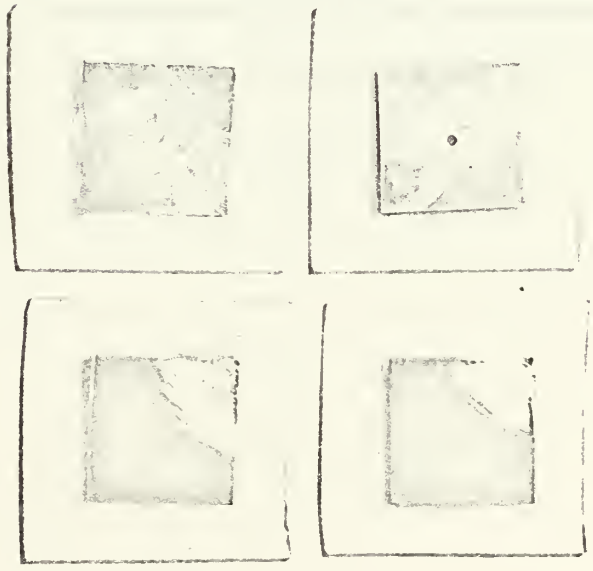

Pumps used in static tests.

Figure II-4

The explanation of this break is not certain. It is probably the result of an internal circulation of the fluid within the larger diameter pump which results in lower pressure. See figure II-5.

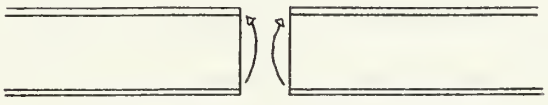

Small Diameter Pump

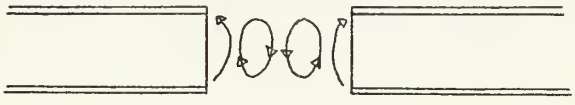

Large Diameter Pump

Figure II-5

Conclusions

The following conclusions are drawn about the static pressure produced by pumps with the proposed geometry of chapter I.

(1) The static pressure is related to the applied voltage by $p = C\epsilon \left(\frac{U'}{\chi}\right)^2$ where C depends upon pump dimensions and freon purity. It is usually in the range 0.8 to 1.1 .

(2) The static pressure at constant voltage takes a sharp drop for pump diameters greater than 1.6 mm if pump length is held constant at 1/16 inch (1.59 mm). It is approximately constant for diameters less than 1.6 mm and decreases slowly after the large drop for larger diameters.

CHAPTER III

DYNAMIC PUMPING

DYNAMIC PUMPING

If the ion drag device is to be used as a pump, the fluid must move, and the mathematical model must take this velocity into account. In this chapter the theory of the last chapter is altered to account for fluid motion. The generated pressure is determined as a function of fluid velocity. Then the hydrodynamics of the pump are investigated and the models combined to give a prediction of total pressure vs. velocity. Measured pressure-velocity characteristics are presented for comparison and it is seen that the theoretical model tends to overestimate the unstable nature of the characteristic.

One Dimensional Dynamic Model

The assumptions of the model for dynamic conditions are similar to those for the static model: charge relaxation time of fluid is greater than pump transient time; liquid appears as a conduction; one dimensional dependence of field and charge density; no influence of lateral boundries.

The model is shown in figure III-2 and the equations to be solved are given in (1) through (4) below. Equation (4) has been altered to account for convective transport of charge. Charge diffusion is again neglected.

	x dependence	
$\nabla \rho = \rho E$	$\frac{d\rho}{dx} = \rho E$	(1)
$E = -\nabla U$	$E = -\frac{dU}{dx}$	(2)
$\nabla E = \frac{\rho}{\epsilon}$	$\frac{dE}{dx} = \frac{\rho}{\epsilon}$	(3)
$g = \rho(Eb + v)$	$g = (Eb + v)$	(4)

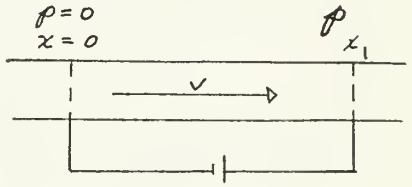

Figure III-1

Solving equations (1) through (4) for $E(x)$ and $P(x)$ yield (5) and (6) below.

$$g = \epsilon \frac{dE}{dx}(Eb + v)$$

$$\frac{g}{\epsilon b} = \epsilon \frac{dE}{dx} + \frac{v}{b}\frac{dE}{dx}$$

integrate $x = 0$ to x, $E = E_o$ to E

$$\frac{g}{\epsilon b}x = \frac{1}{2}\left(E^2 - E_o^2\right) + \frac{v}{b}\left(E - E_o\right) \quad (4A)$$

solve for $E(x)$

$$E(x) = \left[\frac{2gx}{\epsilon b} + \left(E_o + \frac{v}{b}\right)^2\right] - \frac{v}{b} \quad (5)$$

$$\rho = \epsilon \frac{dE}{dx}$$

$$\rho(x) = \frac{q/b}{\left[\frac{2qx}{\epsilon b} + \left(E_o + \frac{v}{b}\right)^2\right]^{1/2}} \tag{6}$$

To connect charge density, electric field, and fluid pressure

$$\frac{d\phi}{dx} = \rho E$$

$$\frac{d\phi}{dx} = \frac{q}{b} - \frac{\frac{Uq}{b^2}}{\left[\frac{2qx}{\epsilon b} + \left(E_o + \frac{v}{b}\right)^2\right]^{1/2}}$$

integrate $x = o$, x and $\phi = o$, ϕ

$$\phi_1 = \frac{\epsilon}{2}\left[\frac{2qx_1}{\epsilon b} - 2\frac{v}{b}\left\{\left[\frac{2qx_1}{\epsilon b} + \left(E_o + \frac{v}{b}\right)^2\right]^{1/2} - E_o + \frac{v}{b}\right\}\right] \tag{7}$$

To introduce voltage, integrate equation (5) using equation (2)

$$-\frac{dv}{dx} = E = \left[\frac{2qx_1}{\epsilon b}\left(E_o + \frac{v}{b}\right)^2\right]^{1/2} - \frac{v}{b}$$

$$-U_1 + U_o = \frac{\epsilon b}{3q}\left\{\left[\frac{2qx_1}{\epsilon b} + \left(E_o + \frac{v}{b}\right)^2\right] - \left(E_o + \frac{v}{b}\right)^3 - \frac{v}{b}x_1\right.$$

(The $\left(E_o + \frac{v}{b}\right)^3$ term was introduced as part of an arbitrary constant.)

The voltage difference $-U_1 + U_o$ will be written as $U - U^*$ where U^* represents the portion of the driving voltage necessary to generate the ions and U is the total voltage across the pump.

$$\frac{U - U^*}{\frac{2}{3}x_1} = \frac{\epsilon b}{2x_1 q}\left\{\left[\frac{2qx}{\epsilon b} + \left(E_o + \frac{v}{b}\right)^2\right]^{3/2} - \left(E_o + \frac{v}{b}\right)^3\right\} - \frac{3v}{2b} \tag{8}$$

To solve for pressure explicitly in terms of voltage it is again necessary to make assumptions as to the value of the electric field (or charge density) at some point in the channel. In chapter II experimental results tended to support the space charge limited model, i.e. the assumption that the electric field is zero at the emitter in the static condition. This assumption again seems reasonable if the fluid is flowing in the positive direction, i.e. in the direction in which the ions tend to drag it. However if the fluid motion opposes the ion direction this assumption is not reasonable especially if the fluid velocity is on the order of $b E$, the ion velocity relative to the fluid. Stuetzer's[2] assumption was that the current density must be zero at the emitter for negative fluid velocity. Pickard[5] introduces a parameter which indicates the value of the electric field at the emitter and includes this parameter in the pressure equation. However the dependence of this parameter upon fluid velocity is not known, and the assumption of Stuetzer represents one specific value of Pickard's parameter.

The following development will make use of assumptions similar to those of Stuetzer[2]. The results will later be compared with experimental results for pressure vs. velocity measurements, an investigation which was not included in Stuetzer's reports. In light of the experimental results, the adquacy of this model for explaining pressure instability will be discussed.

Emitter Field Assumptions

$E_0 = 0 \qquad V \geq 0$

$E_0 = -\frac{V}{b} \qquad V < 0$

From equation (7) for $V \geq 0$

$$\rho_1 = \frac{\epsilon}{2}\left[\frac{2gx_1}{\epsilon b} - 2\frac{V}{b}\left\{\left[\frac{2gx_1}{\epsilon b} + \left(\frac{V}{b}\right)^2\right]^{1/2} - \frac{V}{b}\right\}\right]$$

$$\frac{2\rho_1}{\epsilon} = \frac{2gx_1}{\epsilon b} - 2\frac{V}{b}\left[\frac{2gx_1}{\epsilon b} + \left(\frac{V}{b}\right)^2 + 2\left(\frac{V}{b}\right)^2\right.$$

$$= \left[\left(\frac{2gx_1}{\epsilon b} + \left(\frac{V}{b}\right)^2\right)^{1/2} - \frac{V}{b}\right]^2$$

from equation (4A)

$$\frac{gx_1}{\epsilon b} = \frac{1}{2}E^2 + \frac{V}{b}E = E\left[\frac{1}{2}E + \frac{V}{b}\right]$$

$$= \left\{\left[\frac{2gx_1}{\epsilon b} + \left(\frac{V}{b}\right)^2\right]^{1/2} - \frac{V}{b}\right\}\frac{1}{2}\left[\frac{2gx_1}{\epsilon b} + \left(\frac{V}{b}\right)^2\right]^{1/2} - \frac{V}{b} + \frac{V}{b}\right\}$$

$$= \frac{\epsilon b}{2x_1}\left(\frac{2\rho}{\epsilon}\right)^{1/2}\left\{\left(\frac{2\rho_1}{\epsilon}\right)^{1/2} + \frac{2V}{b}\right\}$$

$$g = \frac{\epsilon b}{2x}\left(\frac{2\rho_1}{\epsilon}\right)^{1/2}\left\{\left(\frac{2\rho_1}{\epsilon}\right)^{1/2} + \frac{2V}{b}\right\} \qquad V \geq 0 \qquad (9A)$$

For $V \leq 0$ from equation (7)

$$\rho_1 = \frac{\epsilon}{2}\left[\frac{2gx_1}{\epsilon b} - 2\frac{V}{b}\left\{\left[\frac{2gx_1}{\epsilon b}\right]^{1/2}\right\}\right]$$

$$\left(\left(\frac{2gx_1}{\epsilon b}\right)^{1/2} - \frac{2V}{b}\left(\frac{2gx_1}{\epsilon b}\right)^{1/2} - \frac{2\rho_1}{\epsilon} = 0\right.$$

$$\left(\frac{2q\chi_1}{\epsilon b}\right)^{1/2} = \sqrt{\left(\frac{V}{b}\right)^2 + \frac{2\rho_1}{\epsilon}}$$

$$q = \frac{\epsilon b}{2\chi_1}\left[\frac{2\rho_1}{\epsilon} + \left(\frac{V}{b}\right)^2 + \frac{V}{b}\right]^2 \qquad V \leq 0$$

To obtain a relationship between pressure and voltage start with equation (8) written as follows:

for $V \geq 0$ $\qquad E_0 = 0$

$$\frac{U-U^*}{\frac{2\chi_1}{3}} = \left\{\left[\frac{2q\chi_1}{\epsilon b} + \left(\frac{V}{b}\right)^2\right]^{1/2}\right\}^3 - \left(\frac{V}{b}\right) - \frac{3}{2}\frac{V}{b}$$

from (7)

$$\left(\frac{2\rho_1}{\epsilon}\right)^{1/2} + \frac{V}{b} = \left(\frac{2q\chi}{\epsilon b} + \left(\frac{V}{b}\right)^2\right)^{1/2}$$

$$\frac{U-U^*}{\frac{2\chi_1}{3}} = \frac{\left[\left(\frac{2\rho_1}{\epsilon}\right)^{1/2} + \frac{V}{b}\right]^3 - \left(\frac{V}{b}\right)^3}{\left(\frac{2\rho_1}{\epsilon}\left[\left(\frac{2\rho_1}{\epsilon}\right)^{1/2} + 2\frac{V}{b}\right]\right.} - \frac{3V}{2b}$$

$$= \frac{\left(\frac{2\rho_1}{\epsilon}\right)^{3/2} + 3\left(\frac{2\rho_1}{\epsilon} + 3\left(\frac{2\rho_1}{\epsilon}\right)^{1/2}\left(\frac{V}{b}\right)^2\right.}{\left(\frac{2\rho_1}{\epsilon}\right)^{1/2}\left[\left(\frac{2\rho_1}{\epsilon} + 2\frac{V}{b}\right.\right]} - \frac{3V}{2b}$$

$$\frac{U-U^*}{\frac{2\chi_1}{3}} = \left(\frac{2\rho_1}{\epsilon}\right)^{1/2} \frac{\left(\frac{2\rho}{\epsilon}\right)^{1/2} + \frac{3}{2}\frac{V}{b}}{\left(\frac{2\rho_1}{\epsilon}\right)^{1/2} + 2\frac{V}{b}} \qquad V \geq 0$$

(10A)

for $V < 0$, $\qquad E_0 = -\frac{V}{b}$

eq. (8) $\qquad \frac{U-U^*}{\frac{2}{3}\chi_1} = \left(\frac{2q\chi_1}{\epsilon b}\right)^{1/2} - \frac{3}{2}\frac{V}{b}$

from (7)

$$\left(\frac{2\rho_1 x_1}{\epsilon b}\right)^{1/2} = \frac{V}{b} + \sqrt{\left(\frac{V}{b}\right)^2 + \frac{2\rho_1}{\epsilon}}$$

$$\frac{U - U^*}{\frac{3}{3} x_1} = \left(\frac{2\rho}{\epsilon} + \left(\frac{V}{b}\right)^2\right)^{1/2} \frac{V}{b} \qquad V < 0 \qquad \text{(10B)}$$

$$\rho_1 = \begin{cases} \frac{\epsilon}{8}\left[\frac{9}{4}\left(\frac{V}{b}\right)^2 - \frac{AV}{b} + A^2\right)^{1/2} - \left(\frac{3V}{2b} - A\right)\right]^2 & V \geq 0 \\ \frac{\epsilon}{2} A^2 \left(1 + \frac{V}{Ab} - \frac{3}{4}\left(\frac{V}{bA}\right)^2\right) & V \leq 0 \end{cases}$$

(11)

In order to visualize these results, it is helpful to normalize the variables as follows:

(a) Pressure will be normalized in terms of the static pressures

$$\rho_n = \frac{\rho_1}{\rho_s} \qquad \rho_s = \frac{9}{8} \epsilon \left(\frac{U - U^*}{x_1}\right)^2$$

(b) Electric field is normalized by defining $\rho_s = \frac{\epsilon}{2} \mathcal{E}^2$ where $\mathcal{E}$ is the average field which would produce the static pressure according to the above equation

$$E_n = \frac{E}{\mathcal{E}}$$

(c) Velocity is normalized to $b\mathcal{E}$, the velocity of ions in static fluid under the influence of the normalizing field

$$V_n = \frac{V}{b\mathcal{E}}$$

(d) Distance is normalized in terms of the emitter-collector spacing x,

$$x_n = \frac{x}{x_1},$$

other normalizing factors follow

(e) Current is normalized to the static current

$$J = \frac{\epsilon b}{2x_1}\,\mathcal{E}^2$$

$$J_n = \frac{J}{J}$$

(f) Charge density is normalized to the charge density at the collector under static conditions

$$R = \frac{\epsilon}{2x_1}\,\mathcal{E}$$

$$\rho_n = \frac{\rho}{R}$$

All normalized (dimensionless) variables are written with a subscript n.

The equations for pressure, current density, electric field, and charge density can be normalized and are summarized as follows:

Normalized Variables

pressure $\mathcal{P}_n = \frac{\mathcal{P}_1}{\mathcal{P}_s}$, $\mathcal{P}_s$ = static pressure = $\frac{9}{8}\epsilon\left(\frac{v-v^*}{x_1}\right)^2$

distance $x_n = \frac{x}{x_1}$, x_1 = distance from emitter to collector

E. field $E_n = \frac{E}{\mathcal{E}}$, $\mathcal{E} = \sqrt{\frac{2\mathcal{P}_s}{\epsilon}}$ (15A)

velocity $v_n = \frac{v}{V}$, $V = b\epsilon$

Current density $g_n = \frac{g}{J}$, $J = \frac{b\rho_s}{\chi_1}$

Charge density $\rho_n = \frac{\rho}{R}$, $R = \frac{\epsilon}{2\chi_1}\mathcal{E}$

Normalized Equations

$$p_n = \begin{cases} \frac{1}{4}\left[\left(\frac{9}{4}v_n^2 + 5v_n + 1\right)^{1/2} - \frac{3}{2}v_n + 1\right]^2 & v_n \geq 0 \\ 1 + v_n - \frac{3}{4}v_n^2 & v_n < 0 \end{cases} \quad (16)$$

$$g_n = \begin{cases} p_n^{1/2}\left[p_n^{1/2} + 2v_n\right] & v_n \geq 0 \\ \left[\left(p_n + v_n^2\right)^{1/2} + v_n\right]^2 & v_n < 0 \end{cases} \quad (17)$$

$$E_n = \begin{cases} \left[g_n \chi_n + v_n^2\right]^{1/2} - v_n & v_n \geq 0 \\ \left(g_n \chi_n\right)^{1/2} - v_n & v_n < 0 \end{cases} \quad (18)$$

$$\rho_n = \begin{cases} \frac{g_n}{\left(g_n \chi_n + v_n^2\right)^{1/2}} & v_n \geq 0 \\ \left(\frac{g_n}{\chi_n}\right)^{1/2} & v_n < 0 \end{cases} \quad (19)$$

Figures III-2 through III-5 show graphical representations of equations (16) through (19).

Figure III-2 shows that the pressure increases to $\frac{16}{9}$ of the static pressure for large positive velocity, and

falls to zero at $v = -\frac{2}{3} b \mathcal{E}$. The current density shown in figure III-3 goes to zero at $v = -\frac{2}{3} b \mathcal{E}$ (which was the original boundry condition) and becomes linearly dependent upon velocity for large V where convection of charge is the dominant transport mechanism.

Electric field and charge density are plotted as functions of position along the channel with the fluid velocity as a parameter. It is seen that for $v > o$ the charge is swept downstream toward the collector. This produces an increased electric field in the vicinity of the collector since we are operating at constant voltage, and the integral of the electric field must remain constant.

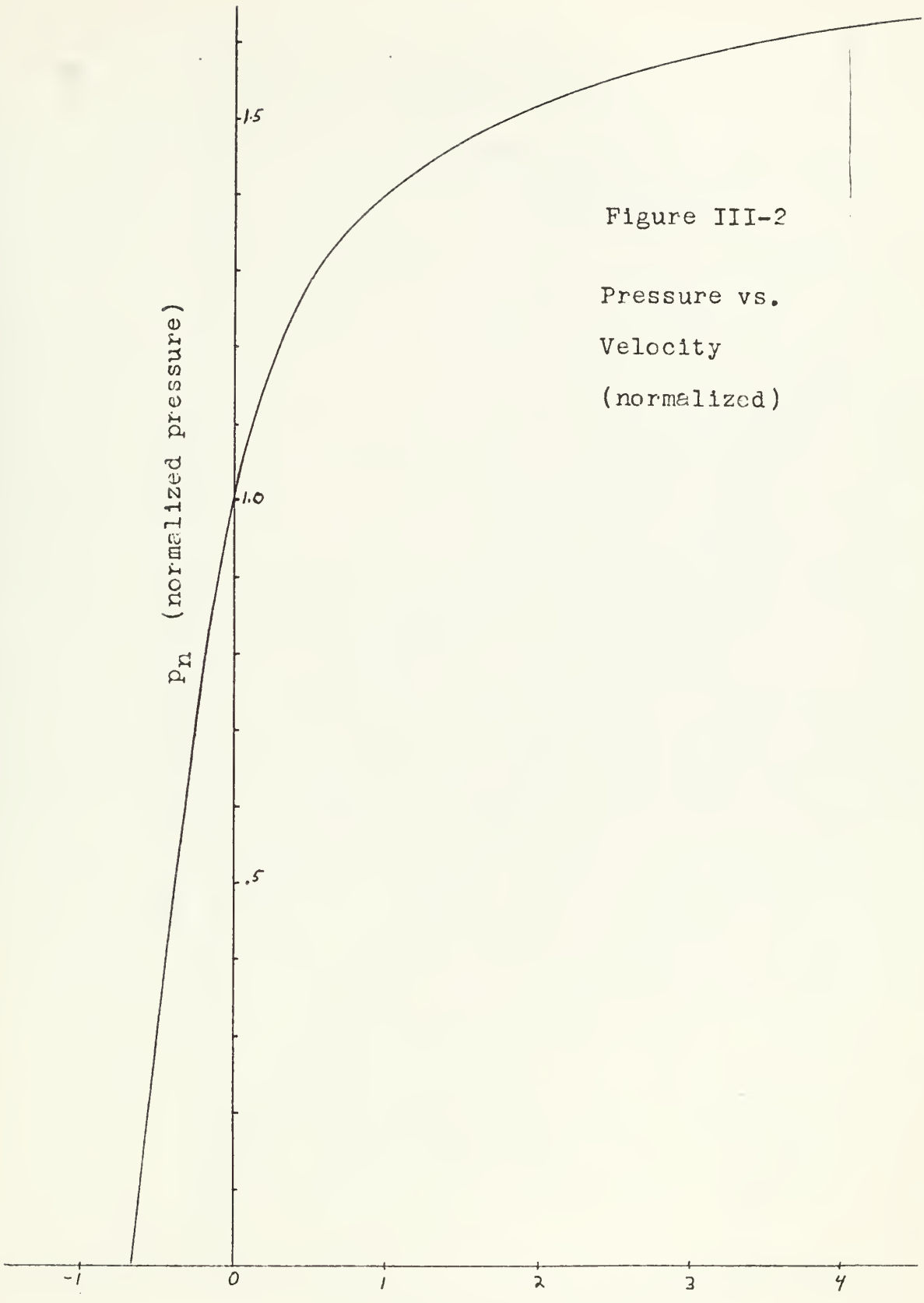

Figure III-2

Pressure vs. Velocity (normalized)

Figure III-3

Current Density vs. Velocity

(normalized)

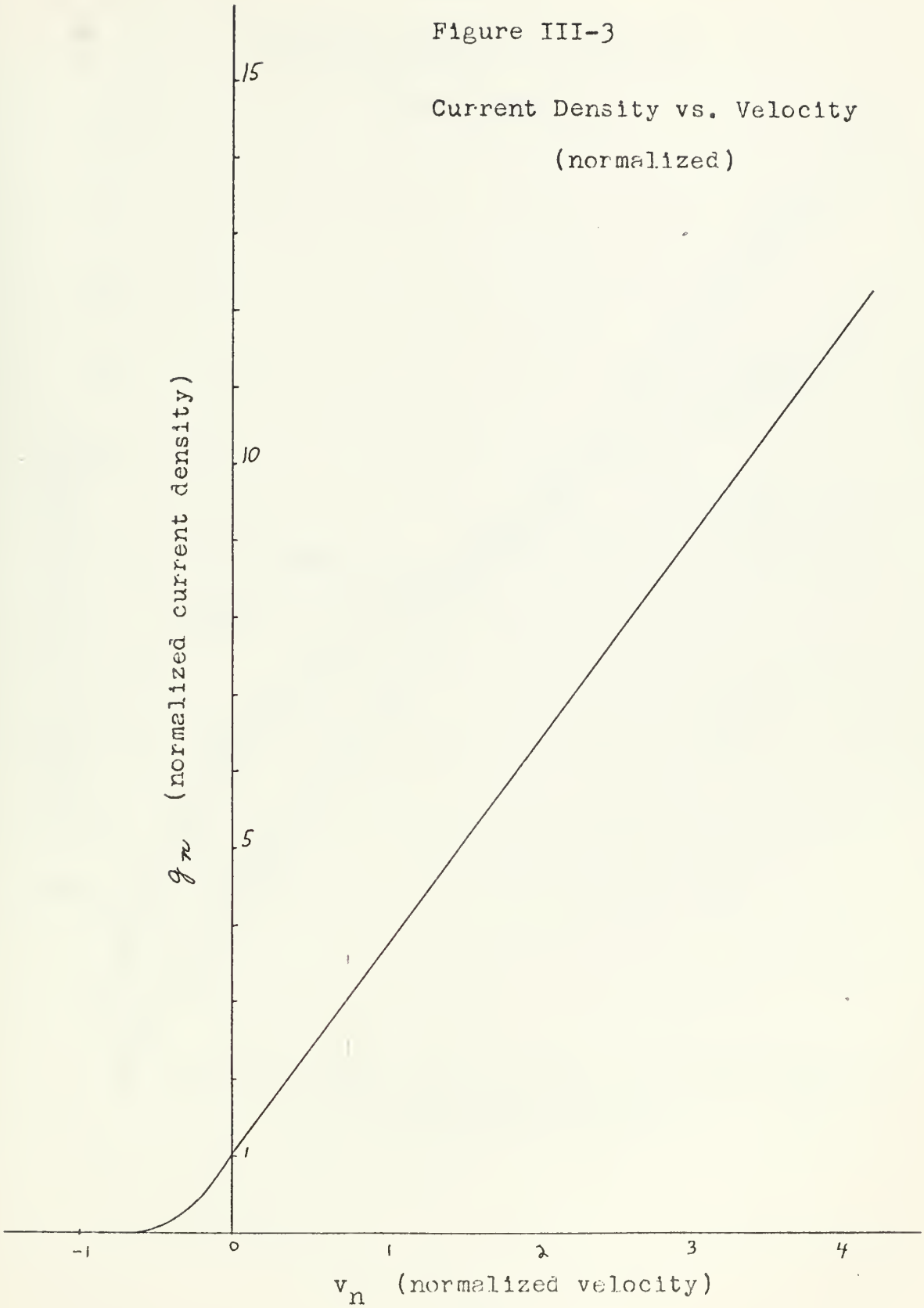

Figure III-4

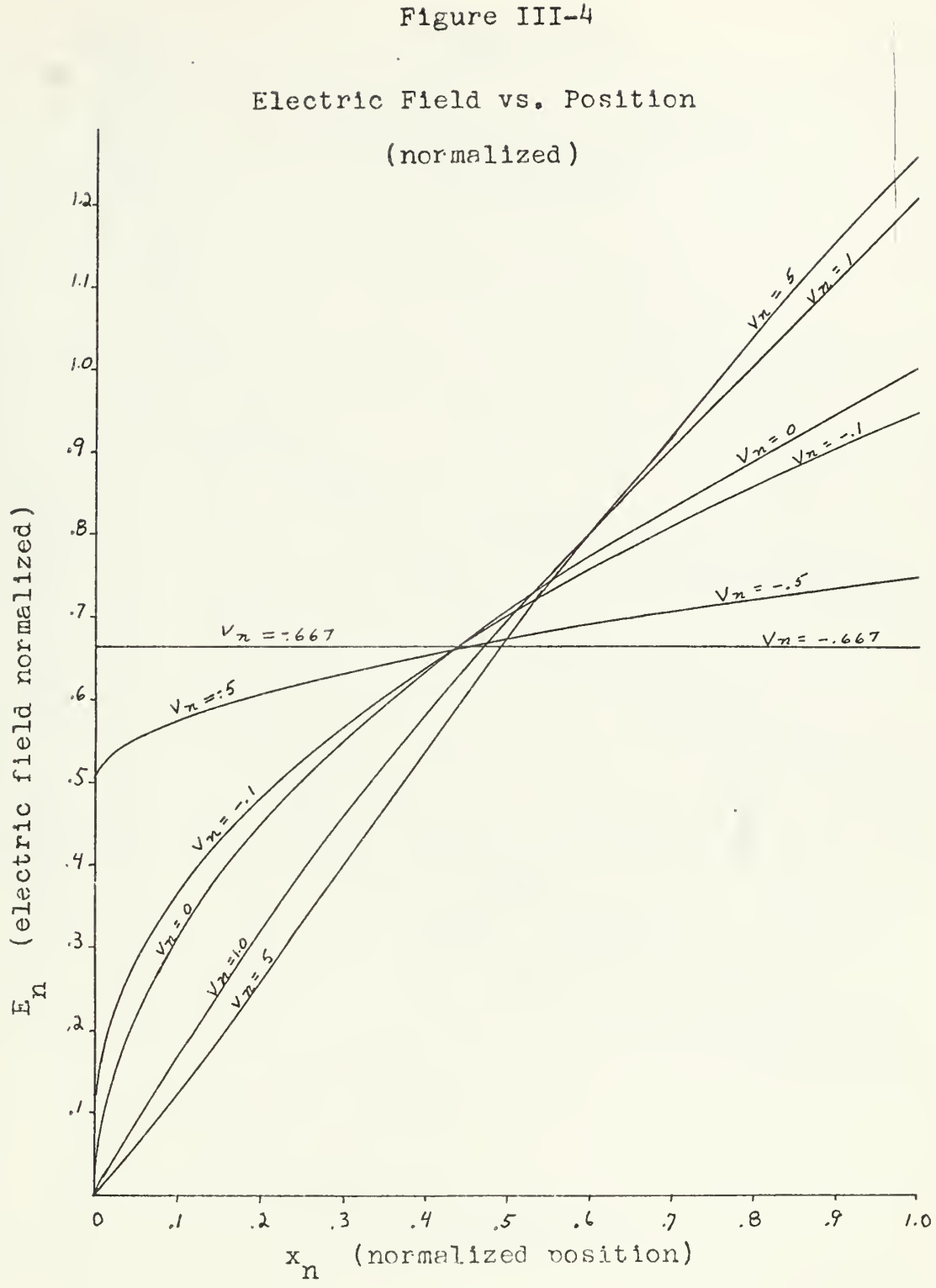
Electric Field vs. Position
(normalized)
E_n (electric field normalized)
x_n (normalized position)
1.2
1.1
1.0
.9
.8
.7
.6
.5
.4
.3
.2
.1
0
.1
.2
.3
.4
.5
.6
.7
.8
.9
1.0
$V_n = 5$
$V_n = 1$
$V_n = 0$
$V_n = -.1$
$V_n = -.5$
$V_n = -.667$
$V_n = .667$
$V_n = .5$
$V_n = -.1$
$V_n = 0$
$V_n = 1.0$
$V_n = 5$

Figure III-5

Charge Density vs. Position

(normalized)

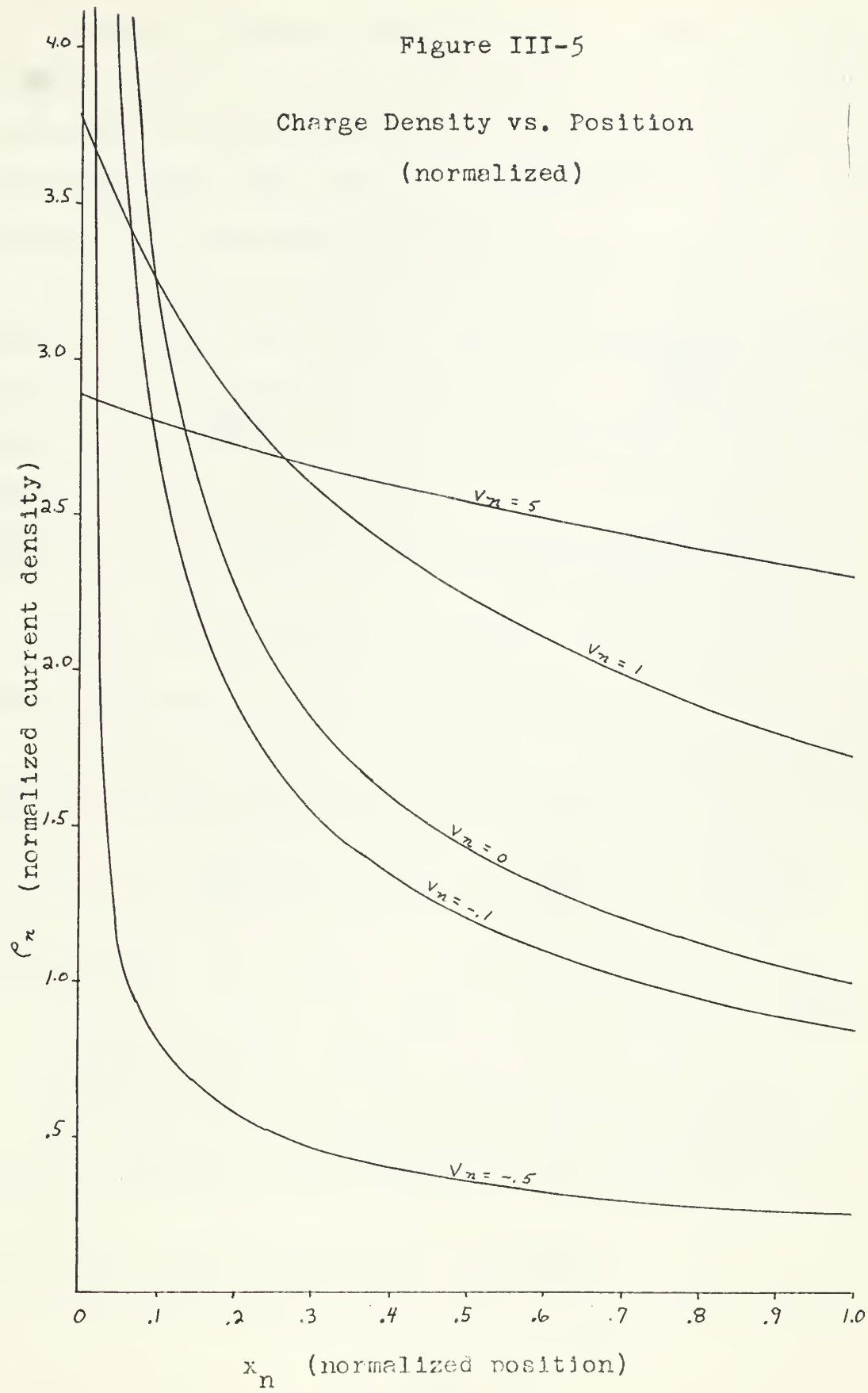

Pressure difference observed across a pump with fluid flowing is due to the generated pressure used minus the hydrodynamic pressure loss due to creation of turbulence beyond the pump. The pump can be modeled as an orifice and analyzed using momentum conservation.

To develop the pressure drop across an orifice we assume that all energy dissipation occurs in the region downstream of the orifice, i.e. between sections 1 and 2. Applying the momentum equation to the dashed control volume of figure III-6.

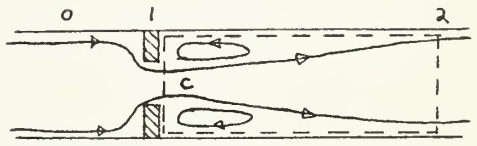

Figure III-6

$$F_{px} = (p_1 - p_a) A_2 = \rho Q (v_2 - v_1) = 0$$

From continiuty

$$Q = v_1 A_1 = v_2 A_2$$

From Bernoulli's equation the head loss is

$$H_{L_{1-2}} = \left(\frac{p_1}{\rho g} + h_1 + \frac{v_1^2}{2g}\right) - \left(\frac{p_2}{\rho g} + h_2 + \frac{v_2^2}{2g}\right)$$

Substituting

$$\frac{H_{L_{1-2}}}{\frac{v_1^2}{2g}} = \left(1 - \frac{A_1}{A_2}\right)^2 \qquad (20)$$

The flow contracts in flowing through the orifice so that the effective area at section c is related to A, by

$A_c = cA$,

Replacing A_2 by cA_2, and using continiuty

$$V_1 c A = v_2 A_2$$

$$H_L = \frac{1}{2g} V_2^2 \left(\frac{A_2}{C A_1} - 1\right)^2$$

or since $Q = V_2 A_2$ (volume flow rate)

$$H_L = \frac{1}{2} g \frac{Q^2}{A_2^2} \left(\frac{A_2}{c A_1} - 1\right)^2$$

The value of c is given expermentally as (8)

$$C = .62 + .38 \left(\frac{A_2}{A_1}\right)^3$$

Putting in dimensionless form similar to equation (16)

$$\Delta \rho_L = \frac{\rho}{2} V_1^2 \left(1 - \frac{c A_L}{A_2}\right)^2$$

$$\Delta p_n = C \frac{(b \varepsilon)^2 v_n^2}{\rho_s} \qquad \text{where } C = \frac{\rho}{2}\left(1 - \frac{c A_1}{A_2}\right)^2$$

$$\Delta p_n = D v_n^2 \qquad D = C \frac{(b \varepsilon)^2}{\rho_s} \qquad (21)$$

The final equation for the pressure difference across a pump is the combination of equation (21) and (16). The pressure difference of equation (21) will always be a loss,

will always be a pressure drop in the direction that the fluid is flowing. Equation (16) does not give a value for the pressure when the normalized velocity is less than $-\frac{2}{3}$, i.e. when the fluid is flowing backwards faster than the

ions are being dragged forward relative to the fluid. The assumption will be made that in this case the generated pressure is zero. The ions are being washed back into the resevoir behind the emitter and probably do not act to exert much pressure rise in the forward direction. The resulting equation is

$$\mathcal{P}_n = \begin{cases} \frac{1}{4}\left[\left(\frac{9}{4}v_n^2 + 5v_n + 1\right)^{1/2} - \frac{3}{2}v_n + 1\right]^2 - Dv_n^2 & v_n \geq 0 \\ 1 + v_n - \frac{3}{4}v_n^2 + Dv_n^2 & -\frac{2}{3} \leq v_n < 0 \\ Dv_n^2 & v_n < -\frac{2}{3} \end{cases} \qquad (22)$$

A plot of equation (22) is shown in figure III-7. The slope of the pressure-velocity curve is positive at $v_n = 0$. This was the basis for Stuetzer's[3] prediction of instability. In the model which he proposed the pressure was not modeled for values less than $v_n < -\frac{2}{3}$. If the same equation as (22) for $\frac{2}{3} < v_n < 0$ is extended to the region $v_n < -\frac{2}{3}$, the pressure will decrease faster than the orifice pressure loss increases, and the pump would not recover from the negative velocity. It is necessary that the pressure-velocity characteristic reverse slope in the negative velocity region, as well as the positive region, to have a pressure oscillation of confined amplitude.

Experimentally Measured Pump Characteristic

The experimentally measured pressure-velocity characteristic is shown in figure III-7. This is for the pump whose geometrical parameters were used in developing the theoretical curve of figure III-7.

It is seen that the slope at $V_n = o$ is positive indicating instability. The measurements were made using an experimental setup as shown schematically in figure III-8. The flow rate was adjusted by changing the valve setting and simultaneous measurements of flow rate and pressure difference across the pump were made. Since the flow was driven by the height of the resevoir, the pump could be reversed in the enclosure and similar measurements taken with negative velocity relative to the normal pumping directions. A picture of the experimental setup is shown in figure III-9.

The measured characteristic does show the positive slope at $V = o$ which is necessary for a condition of unstable pressure. The pump for which these measurements were made oscillated when connected directly to a manometer. The measured characteristic rise for $V > o$ is less than that predicted by equation (22) as is the decrease in pressure for $V < o$.

Figure III-7

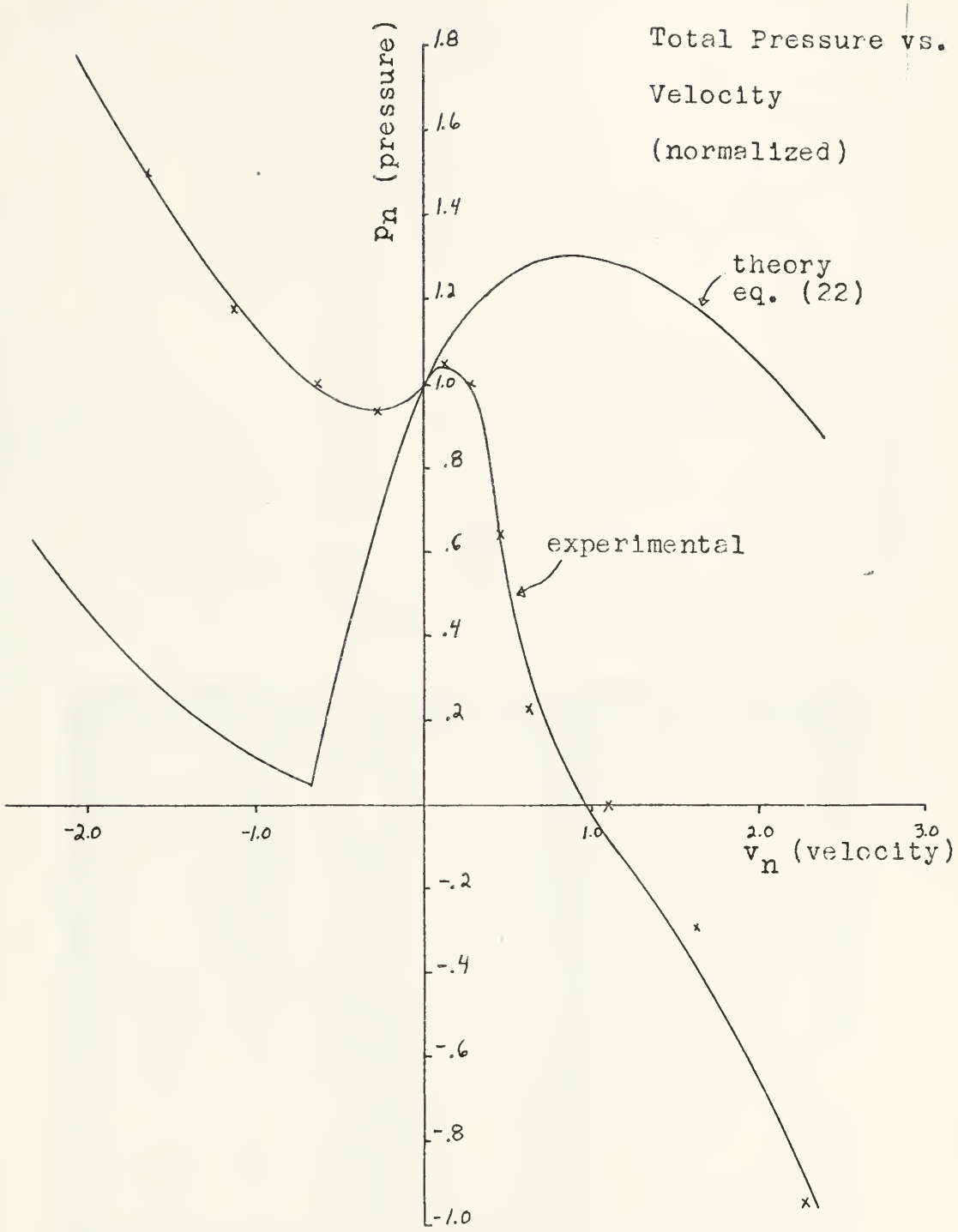
Total Pressure vs.
Velocity
(normalized)
p_n (pressure)
1.8
1.6
1.4
1.2
1.0
.8
.6
.4
.2
-.2
-.4
-.6
-.8
-1.0
theory
eq. (22)
experimental
-2.0
-1.0
1.0
2.0
3.0
v_n (velocity)

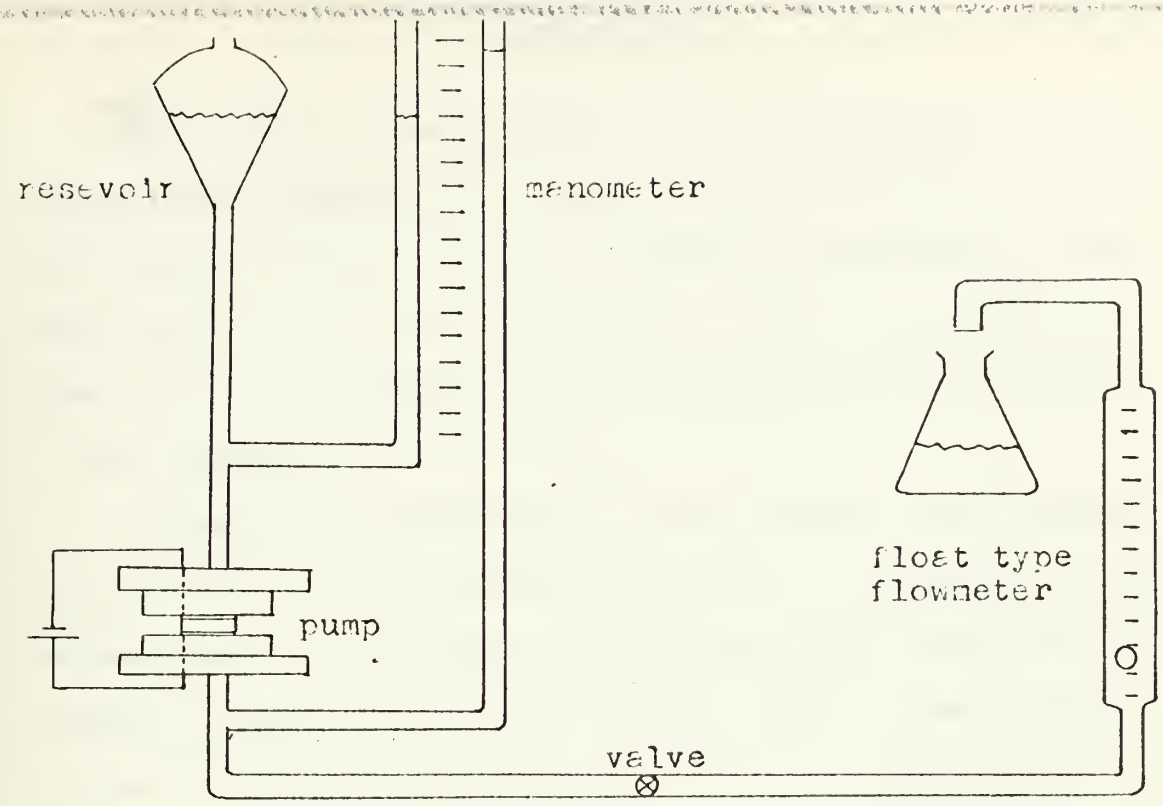

Figure III-9

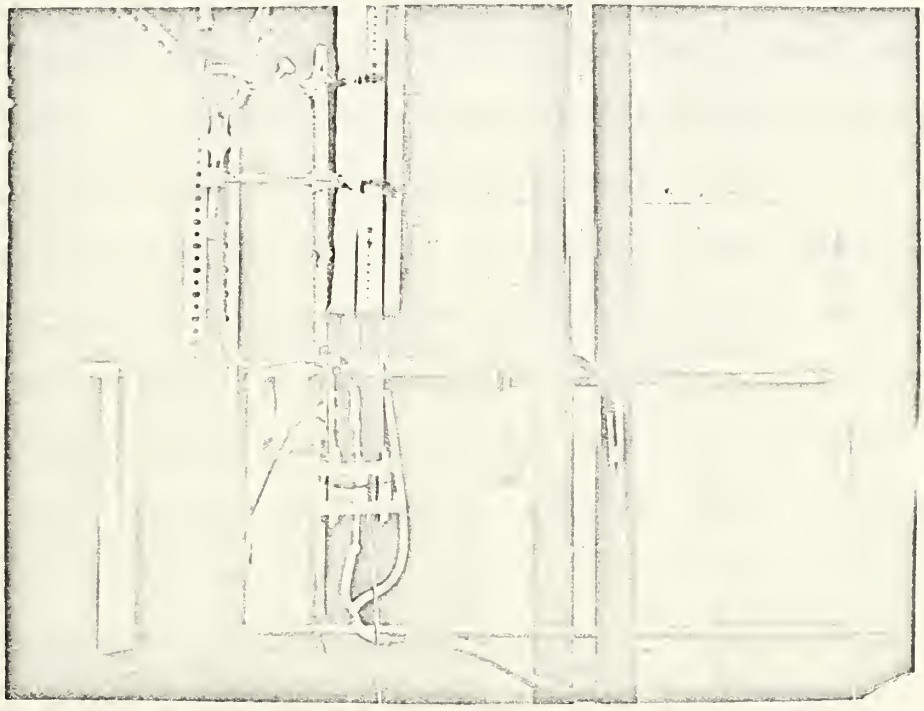

Dynamic pumping experimental setup.

Figure III-10

Conclusions

The forms of the measured pump characteristic tends to support the mathematical model used to develop the theoretical characteristic. The discrepancy in magnitudes of the humps just to the left and right of $V = 0$ can probably be traced to the inadequacy of the boundry condition applied at the emitter.

Although the condition of zero electric field tends to be supported by the evidence presented in chapter II, this assumption does not appear to hold when the fluid has a velocity greater than zero. If the field at the emitter became non zero, i.e. the charge density at the emitter is less than infinite, the generated pressure would fall as shown by Pickard(5). The generated pressure would not rise to a value $\frac{16}{9}$ times the generated pressure at zero velocity, and a smaller pressure rise than predicted by equation (22) for small positive velocity would be exhibited.

For negative velocity it has been assumed that the emitter electric field asjusts itself such that no current passes the emitter in the negative direction, i.e. that the space charge in the vicinity of the emitter continues to build up to produce the required emitter field. If in fact the space charge around the emitter is not this large, the generated fluid pressure would decrease to zero sooner than predicted by the mathematical model and the pressure dip for

velocity slightly less than zero would be less than predicted by equation (22).

There is no way to predict how the emitter boundry condition should change with velocity. A dependence of emitter electric field could be deduced by working backwards from the observed characteristic; however, this would be a circular argument and would add no additional understanding to the problem.

Further evidence of the validity, if not the exact magnitude of the theoretical characteristic is shown by the observed pressure instability. The theoretical implications and experimental observations relative to this problem are presented in chapter IV.

CHAPTER IV

PRESSURE INSTABILITY

Pressure Instability

The discrepancies between measured pressure velocity characteristics and those predicted by the theory of chapter III are discussed in relation to the observed and predicted motion of a pump-manometer experiment. Deficiencies in the model are suggested that may account for these discrepancies, and areas of improvement are suggested.

Pump-Manometer Instabilty

If a pump with the pressure-velocity characteristic of equation (22) chapter III is connected to a manometer a pressure oscillation should result. If the manometer and connecting ducts are must larger than the pump opening, it can be assumed that all hydrodynamic losses occur at the pump orifice and have already been included in equation (22). The difference of level of the fluid in the manometers is y and will have a static value dependent upon voltage and the pump diameter as presented in chapter II. The differential equations describing the motion of the fluid in the manometers are

$$\frac{m_f}{A_m}\frac{dv}{dt} = -\rho g y + p(v_p)$$

$$\frac{dy}{dt} = v$$

where m_f is the mass of the fluid in the manometer, A_m is the cross sectional area of the manometer, and p is the pressure as given by equation (22) in normalized form. The value of p is a function of the velocity through the pump v_p which is related to the velocity of the manometer fluid level v by

$$v_p = \frac{A_m}{A_p} v$$

The static pressure $p(v_p = 0)$ will balance $\rho g y$ static and the equation can be written as a variation about y static

$$\frac{m_f}{A_m}\frac{dv}{dt} = -\rho g(\Delta y) + \Delta\phi(v_p)$$

$$\frac{d(\Delta y)}{dt} = v \qquad (1)$$

If equation (1) is divided through by the velocity it can be written in the form

$$\frac{dv}{dy} = \frac{\frac{A_m}{m_f}\left(-\rho g y + \phi_s \phi_n(v_p)\right)}{v} \qquad (2)$$

where ϕ_n is given by equation (22) of chapter III. The function $\phi_n(v_p)$ satisfies the requirements for the existance of a limit cycle as the solution to equation (2), and this solution can be determined by the use of a graphical technique of Lienard[6].

Experiment

A pump-manometer experiment as shown in figure IV-1 with the dimensions given in table 1 was conducted. Using this data, equation (2) becomes

$$\frac{dv}{dx} = \frac{-7.05x + 53.5\phi_n}{v} \qquad (3)$$

where v is in $^{cm}/_{sec}$ and x in cm. The characteristic 53.5 on is plotted in figure IV-2 using equation (22) of chapter III. Viscous effects and other hydrodynamic resistances were found to be negligible compared to the pump

orifice loss. Superimposed upon the characteristic is a plot of the graphically determined limit cycle.

The amplitude of the oscillation predicted by this cycle is approximately 14 cm with a period of 12.5 seconds.

A plot of the one period of the motion actually observed is given in figure IV-3. The oscillation amplitude is approximately 3 cm with a period of 4.6 seconds.

The experimental pump characteristic given in chapter III figure III-8 was measured for the same pump sometime after the motion of figure IV-3 had been recorded. Electrical breakdown in the pump had by this time degraded its performance somewhat. In figure IV-4 the measured characteristic is plotted and the same limit cycle techniques applied to determine the motion. The predicted amplitude by this graphical construction is 1.5 cm. The observed oscillations at the time the characteristic was measured had an amplitude of approximately 1.2 cm.

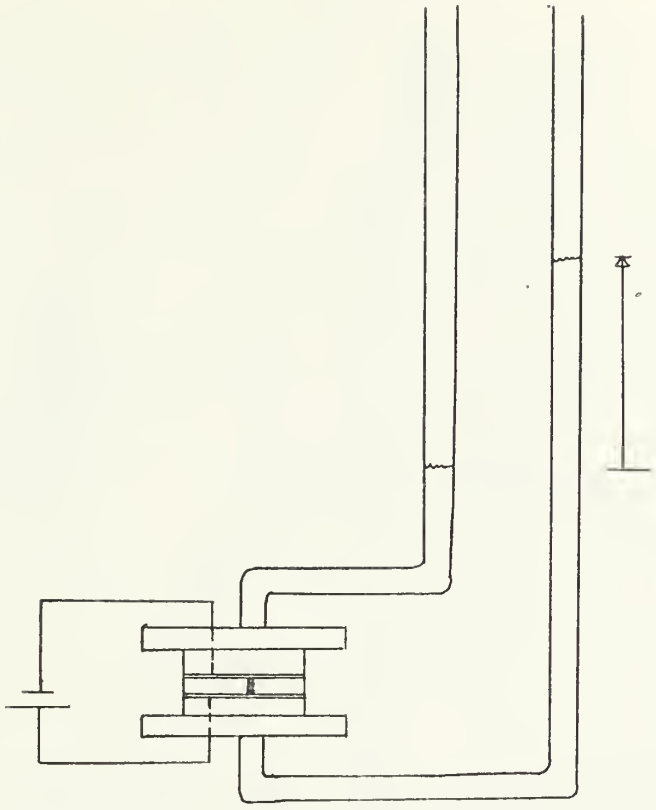

Pump-manometer oscillation experiment.

Figure IV-1

Pump Diameter	.79 mm
Manometer Area	.18 cm^2
Fluid Mass	.04 kg
Static Head	7.60 cm
Electrode Spacing	1.59 mm
Mobility	.39 x 10^{-7}

Pump-manometer dimensions

Table 1

Figure IV-2

Velocity vs. Position

(limit cycle plot)

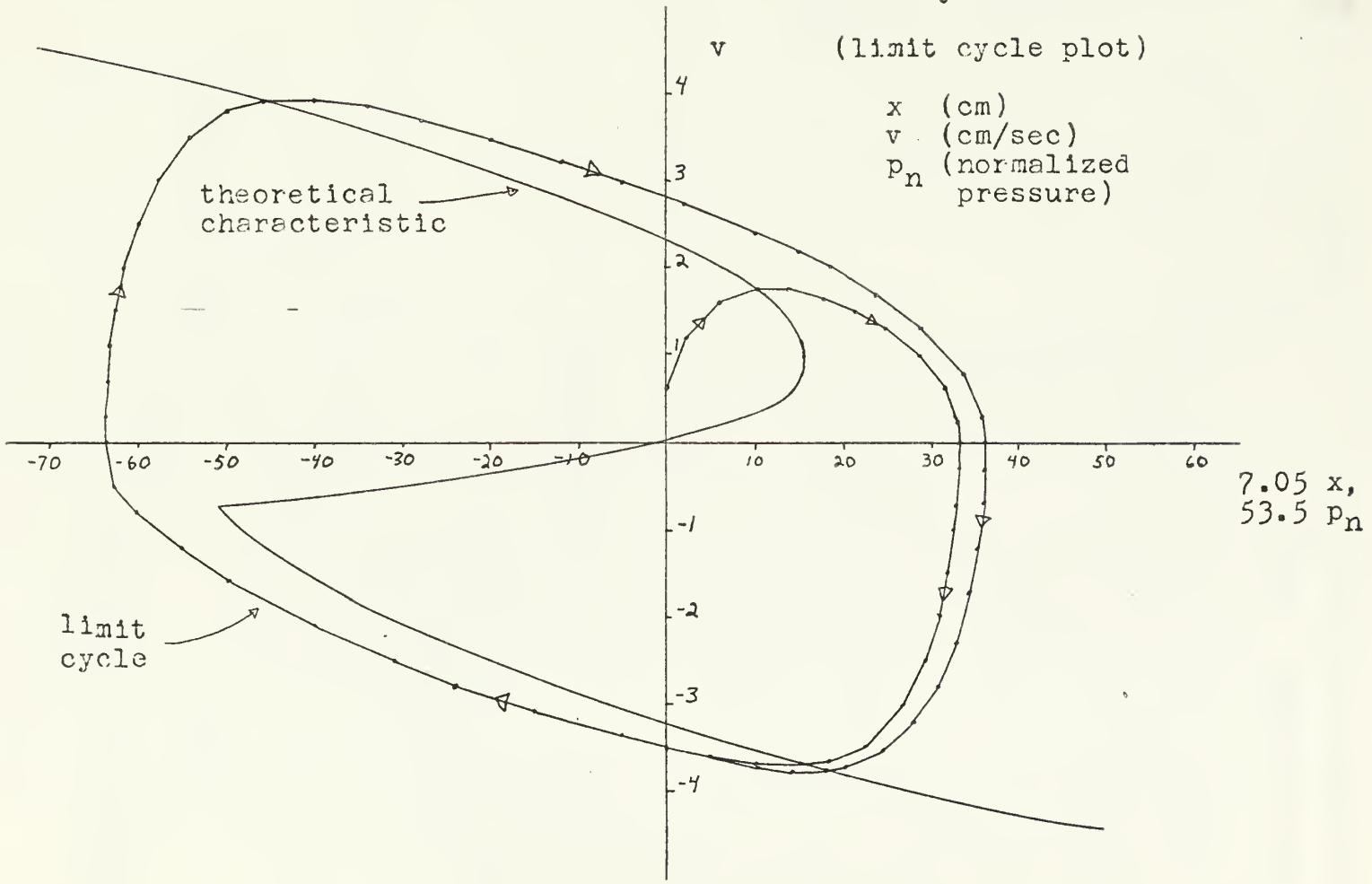

Figure IV-3

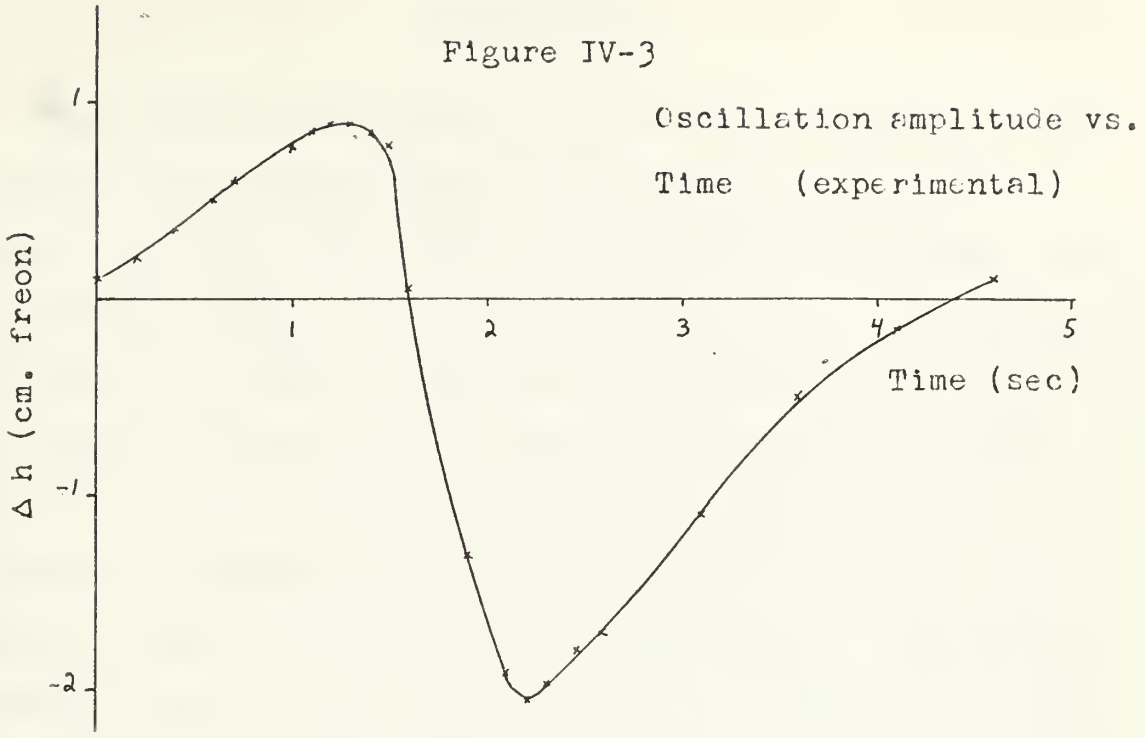

Figure IV-4

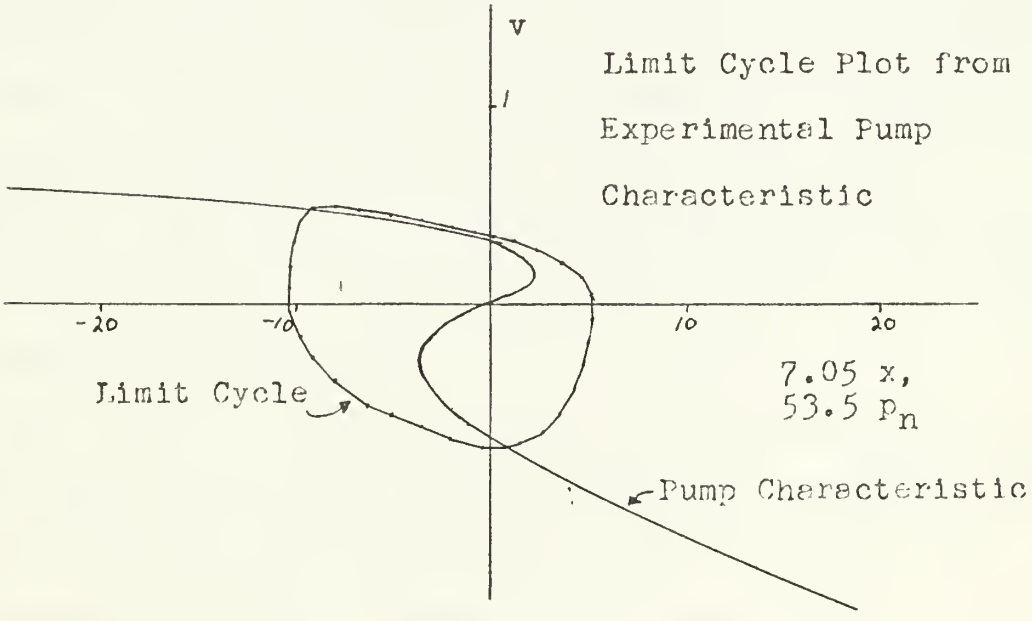

Conclusions

The pressure oscillation amplitudes calculated on the basis of the measured pump characteristic are very nearly equal to the observed amplitudes. This indicates that the mechanism causing the instability is increase in generated pressure for positive velocity as predicted by the theory of chapter III and given in equation (22) of chapter III. The introduction of an additional load in the manometer system by clamping one of the tubes to a very small cross section caused the oscillation to stop and the pressure to assume a steady value. The effect is to introduce viscous loading which eventually causes the characteristic to assume a negative slope at velocity equals zero, i.e. a stable condition.

It had been suspected earlier in this investigation that the mechanism of the instability was a bulk instability in the fluid. Evidence of such a bulk instability in the form of changes in current at critical voltages is given in chapter V. The onset of this apparent bulk instability is at a voltage below the operating point at which the pressure oscillations were observed.

The discrepancies in amplitude of the oscillations from those predicted by theory are the result of the smaller humps in the measured pump characteristic. The comments in the conclusions section of chapter IV apply here again.

CHAPTER V

CHARGE TRANSPORT

Charged Particle Motion Within The Fluid

The experimentally determined curves of current vs. voltage squared shows a very definite break in slope. This suggests that at this point there is a change in the mechanism of charge transport or a change in the number of charged particles being produced. The possibility of the onset of an instability in the bulk is investigated by looking at the ratio of electrical forces induced by the motion to viscous dissipating forces (electric Hartmann number) where the break is observed.

Figure V-1 shows a plot of current (microampers) and static pressure head vs. voltage squared. The current appears to be proportional to voltage squared in two regions with a much larger slope in the region $U^2 > 120\ (KV)^2$. The pressure also has a slight break in slope at approximately the same point.

A possible explanation for this break is the onset of a bulk instability within the fluid occuring at the voltage where the break occurs. The criterion for the onset of such a bulk instability is the relative magnitudes of viscous dissipating forces in the fluid and electrical forces induced by virture of the fluid motions.

Figure V-1

Current, Pressure vs,

Voltage squared

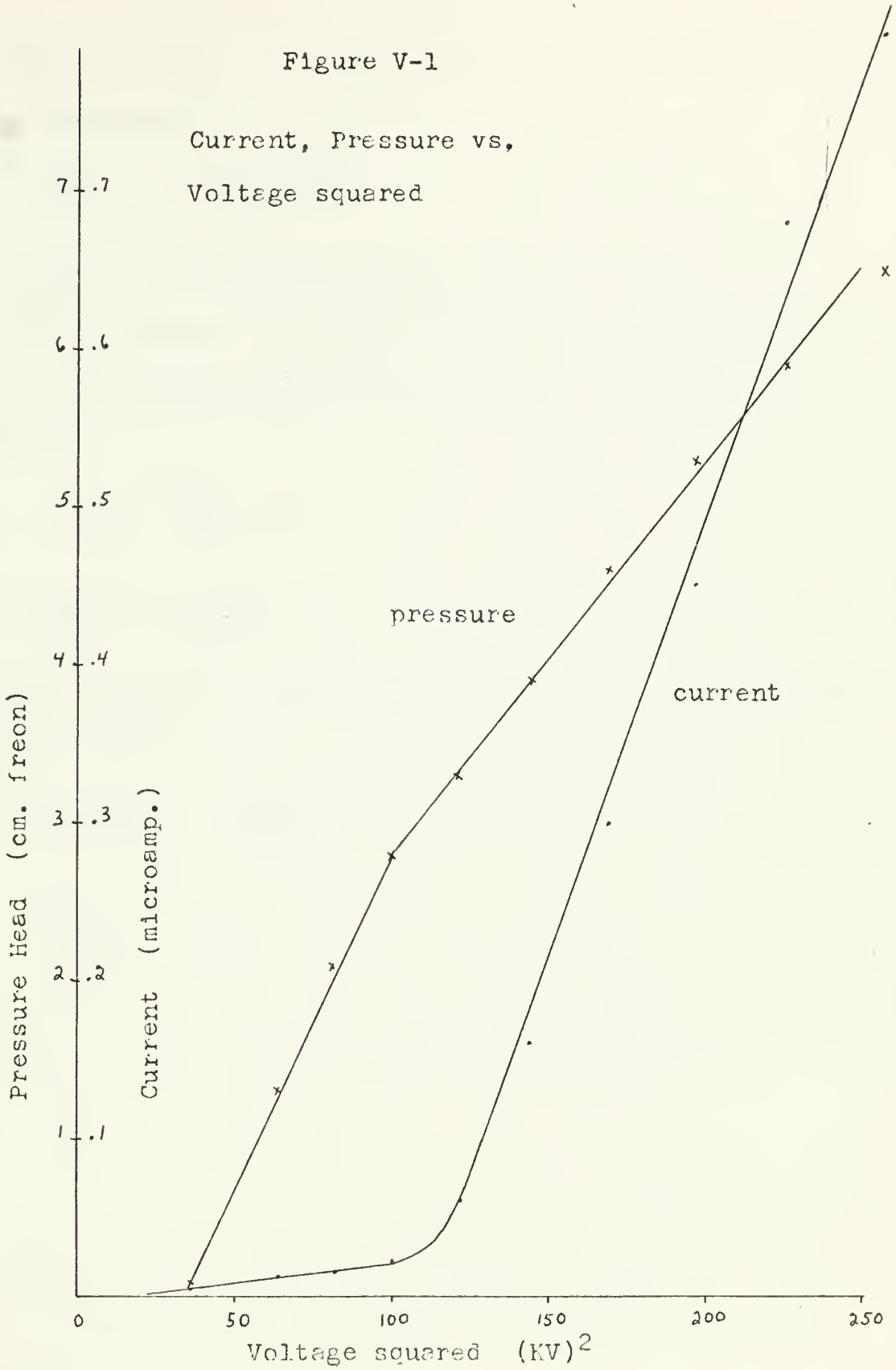

From equation (22) chapter III (with normalizing variables reinserted)

$$\left.\frac{d\phi}{dv}\right|_{V=0} = \frac{\epsilon}{2b}\sqrt{\frac{2\phi_s}{\epsilon}}$$

where $\sqrt{\frac{2\phi_s}{\epsilon}}$ is the characteristic electric field.

If we assume a Poiseuille distribution of velocity within the cyclindrical channel the pressure drop across the channel is

$$\Delta\phi = \frac{8\mu}{R_p^2} L_p V$$

$$\frac{d\Delta\phi}{dv} = \frac{8\mu}{R_p^2} L_p$$

For instability the pressure rise due to elect. forces must increase faster than the viscous dissipation rate.

$$\frac{\epsilon}{2b}\sqrt{\frac{2\phi_s}{\epsilon}} > \frac{8\mu}{R_p^2} L_p$$

$$\frac{\epsilon\sqrt{\frac{2\phi_s}{\epsilon}}}{16b\mu} \quad \frac{R_p^2}{L_p} > 1 \qquad (1)$$

From equation (9) chapter II the value of $\sqrt{\frac{2\phi_s}{\epsilon}}$ is derived by measuring the slope of the h vs. U^2 curve.

$$\sqrt{\frac{2\phi_s}{\epsilon}} = \sqrt{2C} \quad \frac{U}{x}$$

For the experiment shown in figure V-1 the value of C is 0.78 and $\sqrt{\frac{2\phi_s}{\epsilon}} = 7.85 \times 10^6$. For this experiment $2R_p = L_p$. The value of b is determined by simultaneously measuring current and pressure vs. voltage squared.

$$h_s = C \frac{\epsilon}{g\rho} \left(\frac{U}{x}\right)^2$$

$$I = C \epsilon b A \left(\frac{U}{x}\right)^2$$

By solving for C in the first equation, using this value in the second equation and solving for b a value of $b = .304 \times 10^{-7} \frac{m^2}{sec\ volt}$ results. (The value given by Stuetzer for freon 113 was 7×10^{-7}.) Using the value $b = .304 \times 10^{-7}$ and $\mu = .7 \times 10^{-3}$

$$\frac{\epsilon \sqrt{\frac{2\rho_s}{\epsilon}}}{16 b \mu} \frac{R_p^2}{L_p} = 191$$

Since $\sqrt{\frac{2\rho_s}{\epsilon}}$ represents an electric field the expression on the left of inequality (1) has the form $\frac{\epsilon U}{\mu b}$ or an electric Hartmann number. Schneider and Watson[9] have shown that the critical value of this parameter for a planar geometry was 99.5 for the onset of the bulk instability. The value of 191 for this experiment is the same order of magnitude and subsequent experiments have shown that in fact the critical voltage for the break in the current-voltage squared curve is practically independent of pump length and transverse dimensions as would be implied by the form $\frac{\epsilon U}{\mu b}$.

For the oscillating manometer experiment described in chapter IV the voltage was above the value at which this current break evidence of bulk instability occurs. It is probable that the pump fluid is nearly always in the turbulent condition produced by a bulk instability, and that this

type of instability is not the mechanism causing the pressure oscillations.

CHAPTER VI

WICK DESIGN

Design Parameters

The objective of investigation of the proposed ion drag pump geometry was to develop enough information about their performance that an electrohydrodynamic wick could be designed using arrays of these pumps. In order to produce an operable wick the design parameter which must be supplied are

(1) Electrode thickness

(2) Electrode spacer thickness

(3) Pump hole diameter

(4) Pump spacing within an array

(5) Spacing of the arrays relative to each other

As stated previously, the thickness of electrodes has little effect upon pump performance. For most experimental studies brass with thickness .021 inches was used. The more important influence upon performance is the size of burr produced in drilling which depends upon electrode hardness, bit sharpness, and rotational speed of the drill. A burr which protrudes approximately .2mm from the electrode surface seems to work well.

Electrode spacing for most experiments was achieved with 1/16 inch plexiglass between the electrodes. This spacing was found to be best with readily available stock plexiglass and was the result of two considerations:

(a) Smaller spaces such as 1/32 inch plexiglass often resulted in electrical breakdown at very low vol-

tages. This probably because the spacing is becoming almost as small as the burr projection. Since the burr varies from one pump to another the probability that a portion of the burr may extend across the spacer at some point is high and breakdown is quite likely;

(b) Larger spaces such as 1/8 inch require that the voltage be doubled to produce the same generated pressure in the pump. Voltages result (25-30KV) which may cause breakdown outside the pump, and were not as easily produced because of available power supplies.

Pump hole diameter selection should be the result of a tradeoff between higher generated pressures for smaller diameter pumps, and lower hydrodynamic losses in the pump itself for larger diameter holes. However the experimental investigation of generated static pressure vs. hole diameter presented in chapter III clearly indicates that the optimum region of operation is with diameter just below 1.6mm. This insures that the pump will operate with the higher generated pressures just above the break in the curve.

Spacing of holes within an array should be as close as possible to deliver the maximum flow rate with the smallest wick, and to reduce hydrodynamic losses as much as possible. The effect area seen outside the orifice (area A_2 in equation 20 chapter III) becomes less if the pumps are placed closer

together and the orifice losses are consequently less. The factor which determined how close together the pumps could be placed was drill accuracy which required that the center to center spacing be about two diameters. Closer spacing might result in cracks in the material between the holes even if more accurate positioning of the drills were employed. No larger effect upon generated pressure was observed with spacings which varied from 2 diameters to 20 diameters.

Spacing of pump arrays relative to one another is dependent upon the pressure head which is maintained at the flow rate at which the array is operated. For wick operation it is only necessary that one stage lift the fluid vertically through the next stage above it. The usual objective of experiments was to operate at a flow rate such that approximately 1.5 centimeters head was developed. Spacing of arrays approximately one centimeter apart insured that each array would be able to deliver the fluid to the next stage. Very close spacing will result in some backwards drag of ions and a pressure loss between stages. This effect is minimum because of the open reservoirs between arrays. The ions are not directed to give maximum drag effect as they are in the pumps. If a spacing of at least $\frac{1}{4}$ inch is maintained between arrays, the pressure loss is negligible.

An Experimental Wick

A wick of 3 arrays was constructed as shown schematically in figure VI-1. Pictures of the arrays and the assembled wick are in figure VI-2.

The wick dimensions were as follows:

Number arrays	3
Number of holes per array	25
Hole diameter	1.40 mm.
Center to center hole spacing	3.0 mm.
Array electrode spacing	1/16 inch
Electrode thickness	.021 inch
Spacing between arrays	3.5 cm.

The spacing between arrays 3.5 centimeters to permit observation of the flow and possible electrical breakdown if it took place in any of the pumps. A spacing of 1 centimeter would have been more than adequate to isolate the electrodes of adjacent arrays.

Performance

The array was tested using freon doped with copper naphenate at two voltages. At 10 kilovolts the static pressure developed was 5.9 centimeters head. With the load valve opened such that the flow rate was 2.1 cm^3/sec, the pressure was 4.5 cm head. The flow rate of 2.1 cm^3/sec was the maximum reading on the flow meter used; however by de-

creasing the load and pressure across the load larger flow rates were possible. At 12.5 kilovolts the pressure at zero flow rate was 24.6 centimeters and the pressure at 2.1 cm^3/sec flow rate was 22.8cm.

Evaluation

Based upon the above wick experiment along with several other similar experiments the following conclusions are drawn:

(1) Large flow rates can be achieved by building wick arrays with many holes in parallel.

(2) The pressure generated across the arrays is more than sufficient to raise the fluid to the next array above it. Enough arrays placed in series hydrodynamically (and in parallel electrically) can raise the fluid to any arbitrary height.

(3) Pumps have been operated for several hours without noticeable deterioration if the voltage is kept low enough to prevent electrical breakdown.

(4) The pump configuration proposed in chapter I is extremely simple to fabricate. Satisfactory pump arrays can be produced without special care and with a variety of materials.

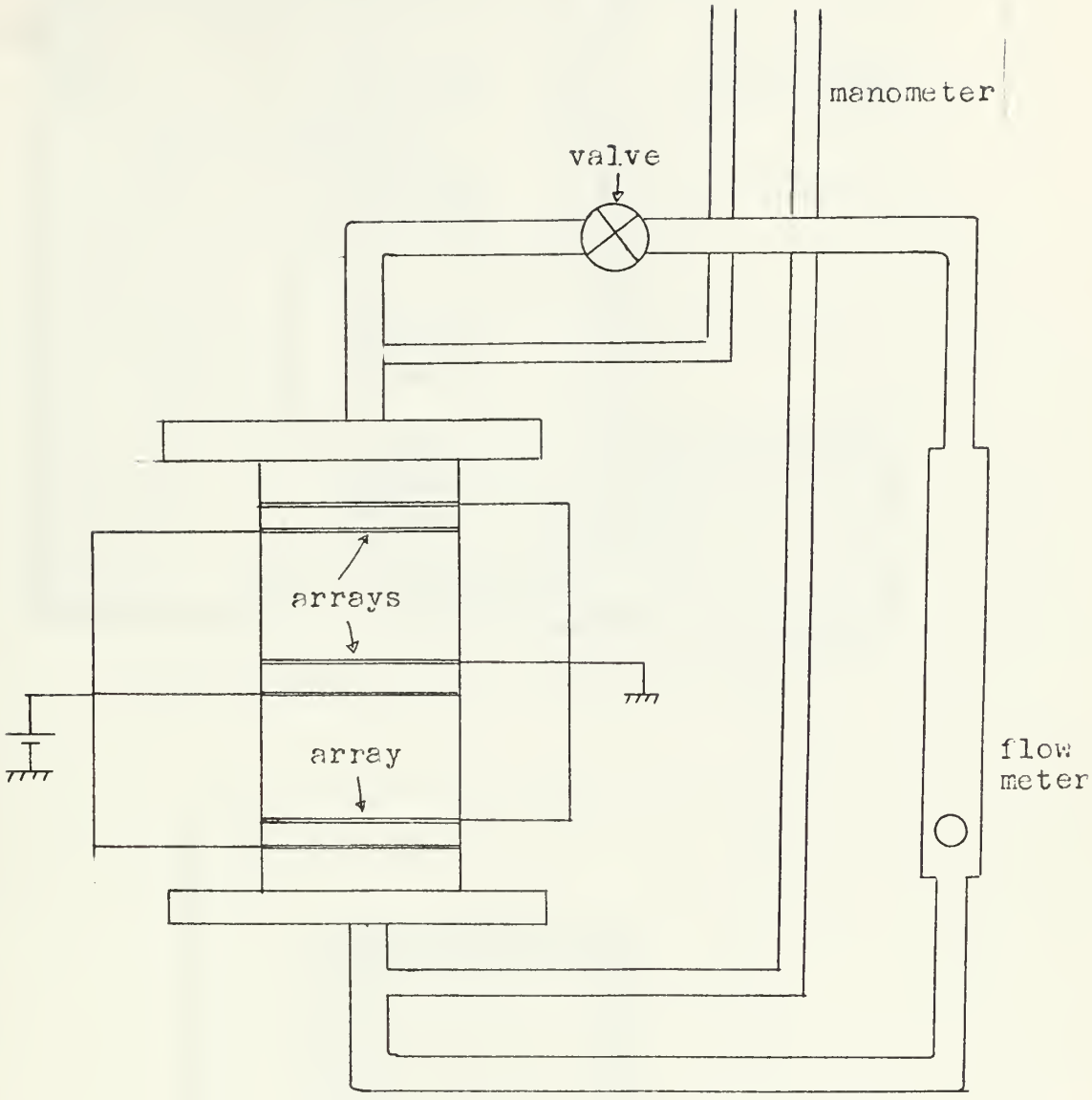

Three array wick experiment

Figure VI-1

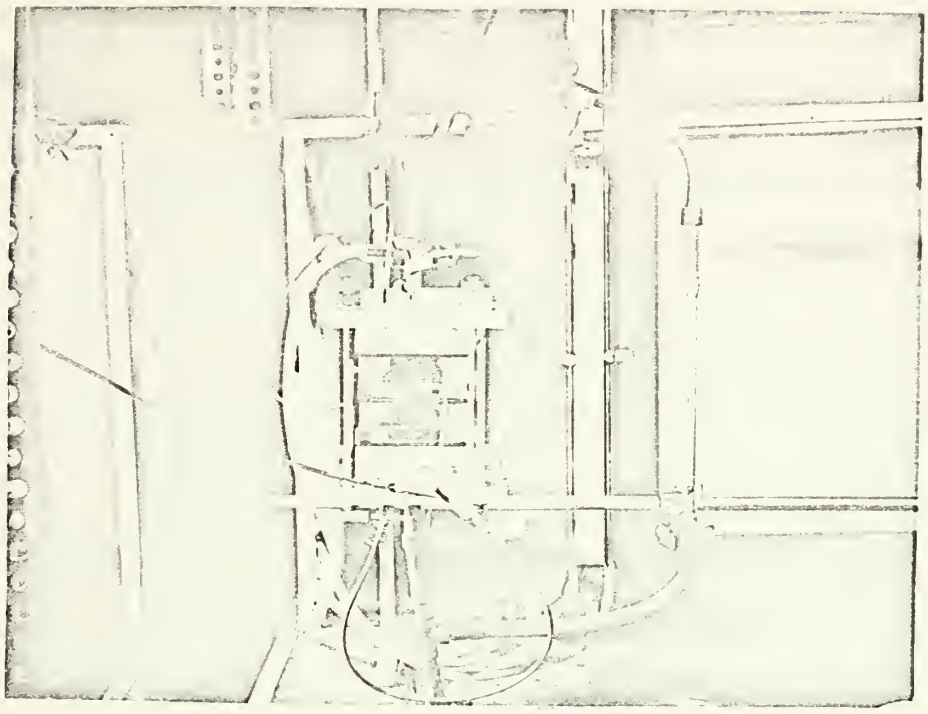

Three array wick experimental setup.

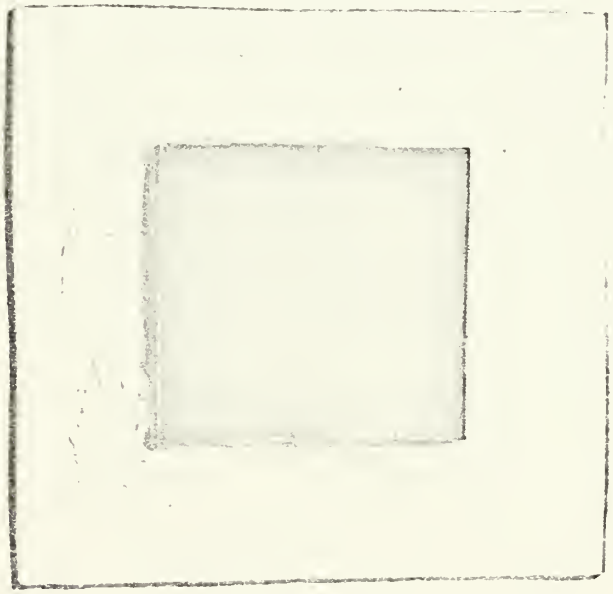

Single array from wick experiment.

Figure VI-2

RECOMMENDATIONS FOR FURTHER INVESTIGATION

Recommendations For Further Investigation

Improvement of the static mathematical model might be investigated by trying to determine the field pattern or a better picture of the charge particle trajectories in the pump. This might be done using an optical technique although the size of the pumps makes this difficult. A set of current measurements at different pump diameters at constant pump length and voltage might reveal more about the possibility of an internal fluid circulation in large diameter pumps as suggested in chapter II.

More accurate-velocity measurements at very small velocity (both positive and negative) should be made and a comparison of motion predicted by this characteristic to recorded motion should be made. Further study of corona emitters in moving liquids might indicate a possible refinement of the emitter field assumption and improve the prediction of the observed experimental characteristic.

Other fluids such as transformer oil should be tested further in the proposed pumps. Some experiments by the author showed that the pumps worked using transformer oil, but extensive experiments were not carried out because of difficultity in cleaning the apparatus for further freon

experiments after using oil. The possibility of using these pump arrays to circulate oil in transformers provides motivation for such investigators.

APPENDIX I

FABRICATION TECHNIQUE

Fabrication Technique

The objective of developing a simple geometry which is easily fabricated is fulfilled by the geometry proposed in chapter I. To insure that the technique used in fabricating the pumps used in experiments reported in this thesis may be reproduced by other investigators or used in constructing wicks for application, the procedure used is described here.

The factor which affects performance of the pump most is the size of the burr which is produced in the drilling process. This depends upon the hardness of the metal plate electrodes used, the sharpness of the drill bits, and the rotational speed of the drill. Thickness of the metal plates seems to have only a very slight effect. Satisfactory pumps were produced with several different brass electrodes and also with aluminum. The thickness of the insulating electrode determines the magnitude of the electric field at a given voltage and therefore the pressure generated. Experience with many experiments showed that a spacer less than 1/16 inch thick tended to arc at low voltages in many pumps because of the irregularities of burrs produced. Hence 1/16 inch insulating spacers were adopted for almost all subquent experiments. Use of this thickness produced satisfactory pumps. For a spacer thickness of 1/16 inch a burr height of approximately 0.2 mm. was found to work well. This may be estimated by inspecting the size of the burr on the electrode from which the bit emerges. The burr produced between the

plates is obviously the one which is desired but inspection of the other one will give indication of size. A very large burr produces by a dull bit may cause the metal electrodes to be too close together inside the hole and produce electrical breakdown at low voltage. A very small burr will not produce charge as well and pumping is limited. However it should again be stated that satisfactory performance can be achieved without an optimum size burr.

Electrode plates were secured to the insulating spacer before holes were drilled. Attempts to drill the holes separately in the electrodes and spacer with allignment afterward were seldom successful and required considerably more effort than securing the electrodes first. The plates and plexiglass spacers were roughened with sandpaper and washed, and the electrodes were glued using epoxy. Typical pumps with single holes for static pressure experiments are shown in figure II-4 along with the enclosure in which they were placed to contain the fluid. Electrical contact was made with the plates by spring electrodes in the enclosure which were connected to an external high voltage power supply. The insulating spacer in the pump sandwiches was extended approximately $\frac{1}{8}$ inch outside the metal electrodes on all sides to prevent arcing outside the pump. Wick arrays with many pumps are shown in figure VI-2 along with the similar enclosure in which they were tested.

APPENDIX II

BIBLIOGRAPHY

Bibliography

(1) Stuetzer, O.M., Journal of Applied Physics, Vol. 30, No. 7, 1959, p.984-994

(2) Stuetzer, O.M., Journal of Applied Physics, Vol. 2, No.6, 1959, p. 642-648

(3) Stuetzer, O.M., Journal of Applied Physics, Vol. 31 No. 1, 1959, p. 136-146

(4) Prandtl, L., Essentials of Fluid Dynamics, Blackie and Son Limited, London and Glascow, p. 168-170

(5) Pickard, W.F., Office of Naval Research Tech. Report No.350,Dec. 1961

(6) Stoker,J.J., Nonlinear Vibrations in Mechanical and Electrical Systems, Interscience Publishers, Inc., p. 129

(7) Jones, T.B., Internal Memorandum No. 159, Continuum Electromechanics Group, M.I.T.

(8) Daily and Harleman, Fluid Dynamics, Addison-Wesley Publishing Co.,Inc.,1966, p.318

(9) Schneider, J.M., Watson,P.K., Proceedings: International Symposium on Electrohydrodynamics, p.74-79